Title
Protein Delivery to Eukaryotic Cells by Engineered Bacteria

Author
Huh, Jin Hang

Publication Date
2012

Peer reviewed|Thesis/dissertation

Protein Delivery to Eukaryotic Cells by Engineered Bacteria

by

Jin Hang Huh

A dissertation submitted in partial satisfaction of the

requirements for the degree of

Joint Doctor of Philosophy
with University of California, San Francisco

in

Bioengineering

in the

Graduate Division

of the

University of California, Berkeley

Committee in charge:

Professor J. Christopher Anderson, Chair
Professor Adam P. Arkin
Professor Francis C. Szoka, Jr.
Professor Daniel A. Portnoy

Spring 2012

Abstract

Protein and DNA Delivery to Eukaryotic Cells by Engineered Bacteria

By

Jin Hang Huh

Doctor of Philosophy in Bioengineering

University of California, Berkeley

Professor J. Christopher Anderson, Chair

Synthetic biologists engineer genetic circuits for applications ranging from biosynthesis to biotherapeutics [1]. Although the application of engineering strategies such as standardization, abstraction, and modularity has long been highlighted as the path to designing complex biological systems [2], early work generally relied on an ad hoc strategy, limiting applications to relatively simple systems [3]. More recently, several groups have explicitly applied modular design to the development of biosynthetic pathways [4], biological computation [5], and increasingly sophisticated logic functions [6]. However, connection of distinct functions to create a useful system-level behavior remains a key challenge [1]. We assessed a possibility and limitation of a modular design when engineering a complex biological system.

By applying a modular design, we engineered E. coli to deliver macromolecules to the cytoplasm of cancer cells in vitro. Fabrication, testing, composition, and troubleshooting of five functional modules produced an efficient system capable of delivering proteins to over 80 % of targeted cancer cells. The modular design strategy enabled facile system modification for both troubleshooting and optimization. These devices were then mixed and matched to build a new type of delivery device that enabled E. coli to escape from the vacuole and secrete payloads. The delivery system was then further modified to deliver payloads to other eukaryotic organisms.

Successful application of modular design to the delivery system demonstrates that abstraction is a simple yet powerful tool for making the design of complex biological systems tractable. We expect that continued refinement of modular design, including incorporation of relevant quantitative information, will enable construction of increasingly complex systems. We envision that the bacterial delivery system developed here may itself become a high level module that can be incorporated into the design of more complex systems, such as a therapeutic bacterium delivering cancer-cell specific microRNA [7].

to my family

Table of Contents

Page

Chapter 1: The payload delivery device

Table of Contents

Page

Chapter 2: The payload secretion device

Table of Contents

Page

Chapter 3: Protein Delivery to Eukaryotic Organisms

Table of Contents

Page

List of Figures

List of Tables

Acknowledgements

I would like to thank my advisor, J. Christopher Anderson, for his patience and guidance throughout my study. I also thank Professor Adam Arkin, Frank Szoka, and Daniel Portnoy for their insightful advice. I thank all of the members of the Anderson Lab for a cooperative and warm working environment, especially Josh Kittleson, Tim Hsiau, Gabe Lopez, and Mariana Leguia for helpful discussion. I thank undergraduate researchers, Berkeley iGEM 2008 and 2010 teams for their hard work: Molly Allen, Christie Brown, Cici Chen, Sherine Cheung, Alex Kim, Amy Kristofferson, Aron Lau, Michael Lu, Conor McClune, Daniela Mehech, Christoph Neyer, Tahoura Samad, Dirk VandePol, Madhvi Venkatesh, and Bing Xia. I thank the King Lab members for sharing their expertise in choanoflagellates, Lillian Fritz-Laylin for *Naegleria*, and Ann Kim and Dan Fletcher for *Dictyostelium*. I thank Bum-yeol Hwang and David Schaffer for helpful discussion on virus, Gavin Price and Steve Ruzin for microscopy, Ann Fischer for providing mammalian cell lines, and Vivek Mutalik for providing basic parts. Finally I thank SynBERC for funding.

Chapter 1

The Payload Delivery Device

1.1 Introduction

Biological engineers have developed genetic circuits to address problems in biosynthesis, biotherapeutics, and biomaterials [1, 8]. However, despite improvements in DNA fabrication capabilities [9], the level of complexity that can be successfully engineered remains limited [3]. In any engineering discipline, the absence of a design strategy eventually hinders progress because the number of components and interactions that have to be simultaneously considered exceeds our capacity. Importantly, biological engineers also lack detailed knowledge about fundamental biological entities and their interactions, further complicating the task of composing more complex systems [10].

Mature engineering disciplines overcome such limitations using a modular design strategy, which involves first partitioning a system into functional units, called modules, and then joining modules to achieve higher order behavior. Modular design limits the number of entities under consideration by reducing arbitrarily large sets of components into a single behavioral specification, and mitigates uncertainty by providing a tractable framework for assessing a variety of module designs and connectivities. While this approach has been employed in the development of biosynthetic pathways [11, 4] and genetic circuits[12], a systematic methodology for engineering biological systems remains elusive.

In this study, we explore the utility of modular design to engineer *E. coli* to deliver macromolecules to the cytoplasm of cancer cells *in vitro*. This problem is of sufficient complexity that it would be inefficient to use *post-hoc* design. Failure or poor performance resulting from construction and testing of the entire system at once would be difficult to troubleshoot. Furthermore, even if the problem were known, the lack of a modular, synthetic infrastructure would hamper replacement of the faulty component with a more effective one. Instead, we divide the system into functional modules, assuming that the modules can be independently fabricated and tested, and that the modules will behave predictably when connected together.

Similar systems have been used for direct modification of mammalian cells [13], delivery of biotherapeutics for cancer and probiotic applications [14] and as a vector for systems where traditional genetic delivery methods are insufficient [15]. Several examples of engineered bacteria have been described based on attenuated *Listeria monocytogenes* and other pathogens [16, 17, 18, 19]. However, use of any attenuated pathogen runs the risk that it will recover or retain uncontrolled aspects of its virulence, rendering this approach infeasible as a general solution.

To address this problem, non pathogenic *E. coli* have been described as a delivery vehicle [20]. This system has been used to deliver functional DNA *in vivo* to airway epithelial cells [21], colonic mucosa [22], and lung epithelial cells [15]. In order to achieve efficient delivery with *E. coli*, the native diaminopimelic acid (DAP) synthesis pathway was mutated to cause dividing bacteria to lyse in the absence of exogenous DAP. However, bacteria persist unlysed inside of lysosomes for over 24 hours [21], likely due to growth stasis in nutrient-limited phagocytic vacuoles. Combined with the operational complexity of continuously providing DAP, this limits the applicability and efficiency of current *E. coli*-based technology. We overcome these limitations by engineering *E. coli* that actively lyse themselves and the phagocytic vacuole in response to the vacuole microenvironment.

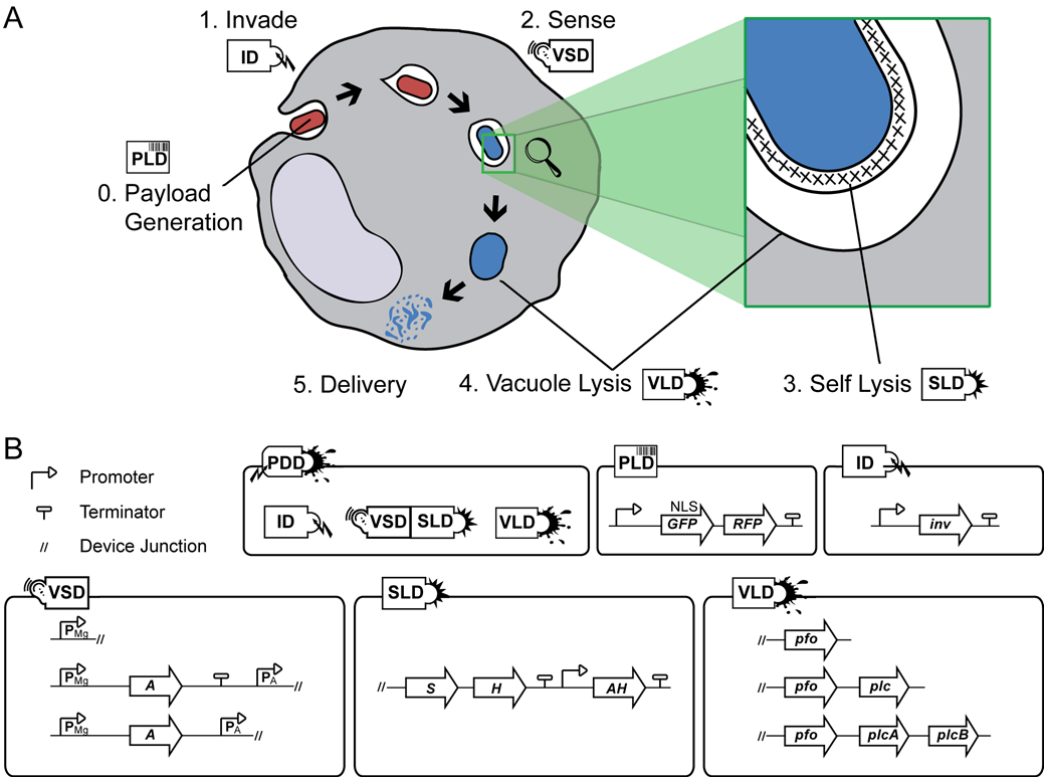

Figure 1.1 Payload delivery scheme and device composition

A. Payload proteins are expressed throughout the delivery process (0). An invasion module causes bacterial uptake into a vacuole (1), where the bacterium responds to the vacuolar environment (2). This triggers self-lysis (3) and subsequently vacuole lysis (4), leading to delivery of the payload to the cytoplasm (5).

B. Composition of devices. PDD: payload delivery device. ID: invasion device. VSD: vacuole sensing device. SLD: self-lysis device. VLD: vacuole lysis device. PLD: payload generation device. *NLS*: nuclear localization signal. *GFP*: green fluorescent protein. *RFP*: red fluorescent protein. *inv*: invasin. PMg: Magnesium responsive promoter. *A*: activator (see supplemental information). PA: Activator responsive promoter. *s*: lysozyme. *H*: holin. *AH*: antiholin. *pfo*: perfringolysin O. *plc*: phospholipase C. *plcA*: phosphoinositide (PI)-specific phospholipase C. *plcB*: phosphatidylcholine (PC)-specific phospholipase C.

1.2 Results

1.2.1 Engineering strategy

Our strategy for payload delivery, illustrated in Figure 1.1A, starts with invasion of the bacterium into the mammalian cell, resulting in bacterial uptake into a vacuole. The bacterium then lyses itself and the vacuole, resulting in delivery of macromolecules into the cytosol. Based on the temporal separation of events, we specified five functional modules necessary to build a complete system: a payload device (PLD) responsible for expression of the payload, an invasion device (ID) responsible for bacterial uptake into the mammalian cell, a vacuole sensing device (VSD) responsible for responding to the vacuolar microenvironment, a self-lysis device (SLD) responsible for bacterial lysis, and a vacuole lysis device (VLD) responsible for rupturing the vacuole. Following the recommendations and examples of others [2, 5, 23], we selected transcription to serve as the interface between modules, providing a versatile junction with readily measured input/output properties. When properly connected, these modules form a complete genetic program for macromolecule delivery. The independent construction and characterization of each device, physical DNA that satisfies the requirements of a module, and the characterization and refinement of interconnected device combinations are described below.

1.2.2 Strategy for measuring transcription

Methods exist for quantifying the number of transcripts produced by a promoter under a particular set of conditions[24], and for measuring the relative strength of promoters across a variety of conditions during steady state growth[23]. However, these procedures are experimentally cumbersome and provide little information about the promoter activity outside of steady state conditions. As an alternative to these procedures, we elected to measure relative transcription. We define relative transcription experimentally as the per cell (OD normalized) fluorescence of bacteria with the promoter of interest driving GFP divided by the per cell fluorescence of bacteria with a standard reference promoter (J23101) driving GFP under a specific set of conditions. By this definition, any two promoters that result in the same per cell fluorescence after a given time period are considered the same, regardless of the temporal dynamics of expression. It is therefore a rough measure of the translational-capacity-normalized, time-averaged transcriptional activity of the promoter. Under conditions where cells are at steady state and have similar growth rates, this equates to the relative promoter units as described before [23]. By using relative transcription, however, we can consider cells under non steady-state conditions. This is essential to predicting the behavior of devices used in the payload delivery system, which functions outside of mid-logarithmic growth.

1.2.3 Independent design and testing of modules

1.2.3.1 Payload device

In order to visually track payload delivery progress from the cytoplasm of extracellular bacteria to the cytoplasm of the target mammalian cell, we constructed a fluorescent protein-based payload. Reasoning that organelle-specific localization of the payload within the mammalian cell would unambiguously indicate successful delivery, we constructed a constitutively-expressed bicistronic operon encoding both untagged RFP and GFP translationally fused to the nuclear localization signal (NLS) of SV40 [25] (Figure 1.1B). Upon release into the mammalian cytoplasm, the RFP should distribute throughout the cytoplasm, while the NLS-GFP should concentrate in the nucleus. By employing this device, we could monitor both the integrity of bacteria and the location of their contents throughout the payload delivery process. The payload device was placed on the plasmid vector carrying spectinomycin resistance gene and pUC origin of replication.

1.2.3.2 Invasion device

Various mechanisms for bacterial invasion of mammalian cells have been described, including the use of invasion [26], a type III secretion system [27], and a surface displayed affibody [28]. The invasin and affibody rely on a specific binding interaction with a host surface protein, while the type III secretion strategy utilizes non-specific protein injection machinery to manipulate the host morphology. In either case, the bacterium is ultimately taken up into a phagocytic vacuole (depicted in Figure 1.1A). Without further intervention, the bacterium is degraded following acidification of the phagosome and progression through a lysosome [29].

Because of its simplicity, we chose a constitutively-expressed invasin, specifically the *inv* gene from *Yersinia pseudotuberculosis*. Invasin binds to ß1-integrins, if present, on the surface of mammalian cells and induces bacterial uptake by Rac-mediated phagocytosis. ß1-integrin is expressed on a variety of cell types [30], although certain tumor cell lines may overexpress it more than others, making them more susceptible targets [31]. In Figure 1.2A, several bacteria bearing the ID have been phagocytosed by a human carcinoma cell (HeLa). This result is consistent with previous work [31], and confirms that the ID independently confers an invasive phenotype.

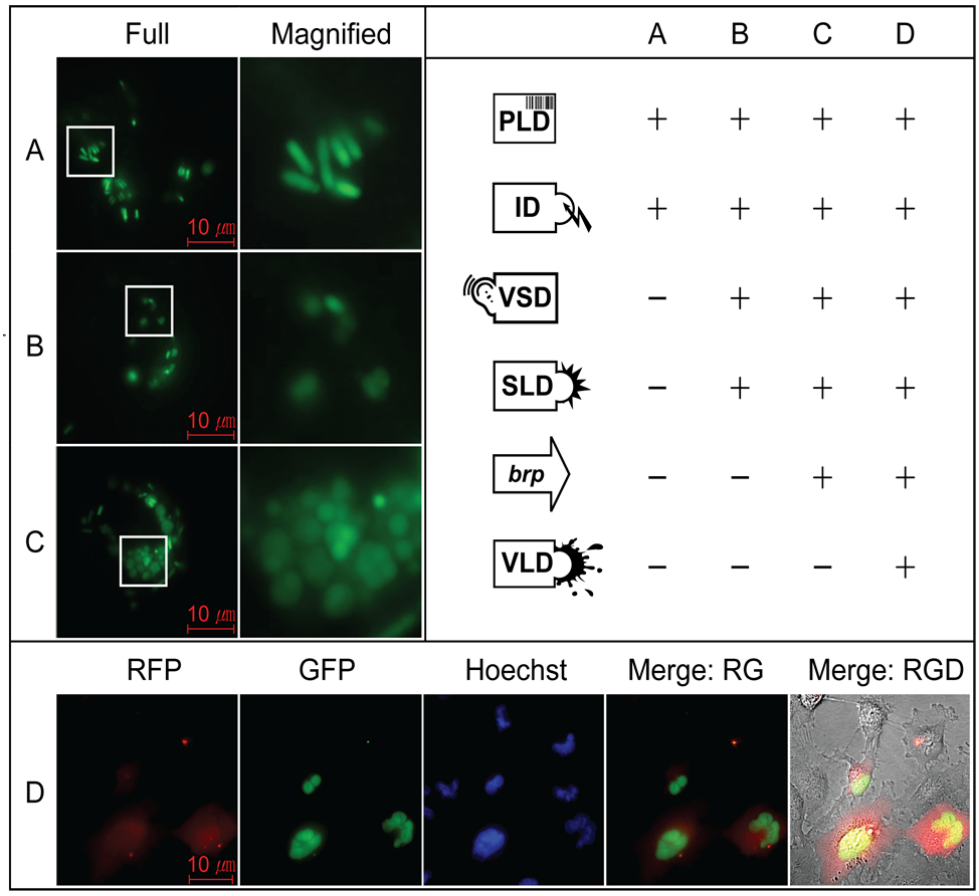

Figure 1.2 Device and system function *in vivo*

E. coli bearing the payload device and one or more other devices were incubated with HeLa (A,B,C) or U373 MG (D) cells and then observed by microscopy. (+) indicates the device is installed, (-) indicates the device is not installed.

A. The ID only.

B. The ID and the VSD(P_{phoP}) driving the SLD(λ) without BRP.

C. The ID and the VSD(P_{phoP}) driving the SLD(λ) with BRP.

D. The ID, the VSD(P_{mgrBl}) driving a SLD(λ) with BRP, and the VLD(degradation tagged *pfo*/*plc*) driven by a constitutive promoter, P_{con}.

1.2.3.3 Vacuole sensing device

The bacterium must be able to sense and respond to uptake into a vacuole to achieve payload delivery and prevent eventual degradation in a lysosome. Thus, the sensing module must differentiate between encasement within a vacuole and both the bacterial and mammalian growth medium to prevent premature self-lysis. A number of prior studies (1 and references therein) have addressed similar problems by coupling changes in specific environmental elements to transcriptional activity.

We reasoned that the lack of ionic nutrients, notably magnesium and iron, could serve as such an environmental cue for the vacuole interior. Therefore, a variety of stress or nutrient-responsive promoters, including those driving *bioB*, *carA*, *iroB*, *fhuA*, and *glgS* from *E. coli* and *spv* from *Salmonella*, were placed in front of GFP, and strain fluorescence measured in different environments. Of the promoters

tested, P_{phoP}, which is regulated by the PhoPQ two-component system, demonstrated the best responsiveness in LB medium (data not shown).

In the PhoPQ two-component system, PhoQ phosphorylates PhoP in response to low concentrations of divalent cations such as magnesium; in turn, phosphorylated PhoP activates transcription of genes responsible for magnesium homeostasis and a variety of other functions in *E. coli* [32, 33, 34]. Based on the behavior of invasive pathogens [35], we reasoned that PhoPQ responsive promoters, likely responding to low Mg^{2+} in the vacuole [36], would serve as an appropriate trigger. We measured the Mg^{2+}-repressed (off-state) and Mg^{2+}-starved activity (on-state) of a known PhoPQ responsive promoter, P_{phoP} (Figure 1.3), confirming its response to Mg^{2+} starvation.

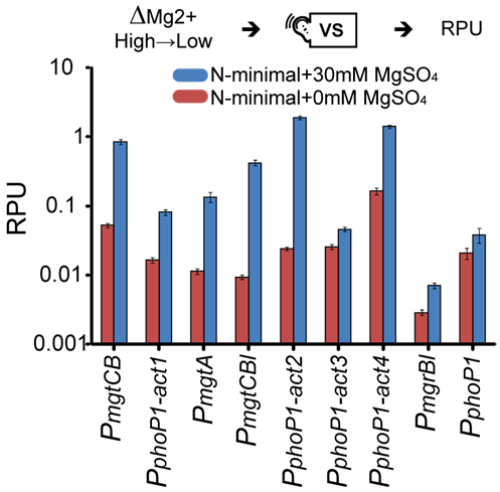

Figure 1.3 Characterization of the vacuole sensing devices
The induced (On) and uninduced (Off) activity of VSD variants. Error bars in both panels are the standard deviation of 4 biological replicates.

1.2.3.4 Self-lysis device

After detecting entry into a vacuole, the bacterium must lyse itself. Lysis strategies of various bacteriophages have been reported, including both multi- and single-gene systems [37]. We elected to test the T4 and lambda lytic systems because we expected their threshold-gated architecture to be more tolerant to leaky basal expression. Antiholin inhibits pore formation by competitively binding to holin. Above a critical threshold, free holin accumulates and forms pores in the inner membrane [38]. Lysozyme then gains access to the periplasm through those pores and degrades the peptidoglycan layer, resulting in *E. coli* lysis.

To build a transcriptionally responsive self-lysis device, we placed antiholin under the control of a weak constitutive promoter, and cloned a promoterless holin and lysozyme expression cassette 5' of the antiholin (depicted in Figure 1.1B). To independently characterize the lambda- and T4-based systems *in vitro*, we connected the arabinose-inducible promoter P_{BAD} to the front of the module.

Figure 1.4 shows the effectiveness of these devices as a function of input relative transcription, measured both in the presence and absence of magnesium to match the conditions used to test the vacuole sensor (Figure 1.4A and B, respectively). Both lambda- and T4-based systems caused ~80% lysis at the highest relative transcription level tested - in the absence of magnesium. However, the lambda system shows minimal lysis, while the T4 system shows ~40% lysis at the lowest relative transcription tested. Consequently, the lambda system was chosen to integrate with other modules. Interestingly, the self-lysis device functioned poorly in the presence of magnesium, with the lambda system achieved only 20% lysis at the highest relative transcription tested. This is consistent with previous observations that lambda phage lacking *Rz* genes fail to lyse host *E. coli* effectively in the presence of divalent cations [39]. Although the precise mechanism of reduced lysis in the presence of magnesium is unknown, it contributes to the stability of the final system since it reinforces the desired behavior of lysis occurring only in the absence of magnesium.

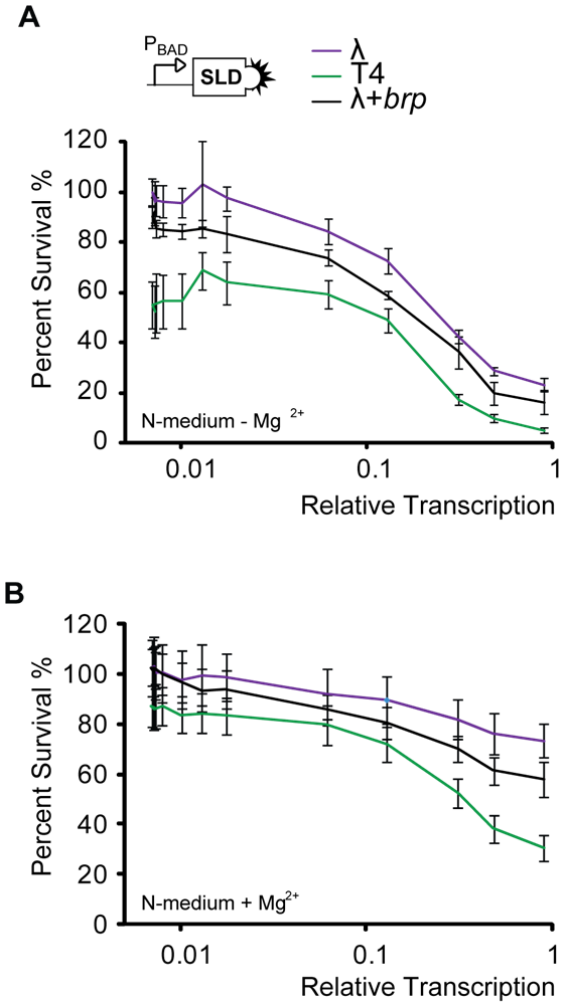

Figure 1.4 Characterization of the self-lysis devices
A. The lysis efficiency of SLD variants in the absence of Mg^{2+}.
B. The lysis efficiency of SLD variants in the presence of Mg^{2+}.
Error bars in both panels are the standard deviation of 4 biological replicates.

1.2.3.5 Vacuole lysis device

Once the bacterium has lysed, the only remaining barrier is the vacuole membrane. Viral peptides [40], viral capsids [41], and artificial peptides [42] have all been reported to lyse the vacuole membrane. However, indiscriminant lysis of bacterial and vacuolar membranes or limited activity in non-acidic conditions precludes their use in a payload delivery system. We instead sought to compose a vacuole lysis device (VLD) with little bacterial membrane lysis activity and high function at neutral pH, reasoning that this would ease overexpression in *E. coli* and maintain payload stability. Additionally, the VLD must leave the host cell intact, either through inactivity in the cytosol of the target host cell or exclusive operation on the vacuolar membrane. We therefore fabricated devices using the cytolysin genes phospholipase C (*plc*) and cholesterol-dependent perfringolysin O (*pfo*) from

Clostridium perfringens [43], and two phospholipase C genes from *Listeria monocytogenes*, plcA and plcB [44] (VLD, Figure 1.1B).

The activity of PFO is limited to cellular membranes containing cholesterol, so bacterial membranes remain intact even when PFO is expressed in *E. coli*. We then added N-terminal degrons [45], which we expect to prevent unwanted cytosolic activity by targeting the proteins for rapid degradation by the ubiquitin-proteasome pathway. The *pelB* export leader sequence was then fused to the N-terminus to direct expressed proteins to the periplasm. The export tag was added to make vacuole lysis biochemically independent of self-lysis. Because we could not contrive of a meaningful *in vitro* experiment to independently test VLD variants, they were only tested upon integration with other devices, as describe below.

1.2.4 Connection and refinement of modules

1.2.4.1 Incorporation of invasion with the vacuole sensing device and self-lysis device *in vivo*

Having implemented individual modules, we proceeded to join them into larger systems, starting with the VSD and SLD. Composition of P_{phoP} with the λ SLD generated a device stable in cells in the presence of Mg^{2+} (Figure 1.5), but that caused cell lysis in the absence of Mg^{2+} (data not shown). Since invasion is not directly coupled to downstream events, but rather acts indirectly through the environment, incorporation of the ID only required physically integrating the device into the genome of the same cell as the VSD and SLD. All other devices except for the payload device were placed on the plasmid carrying p15A origin of replication. However, cells with all three devices failed to completely lyse *in vivo* (Figure 1.2B), instead rounding up but remaining intact. This phenotype suggests that either the Mg^{2+} level is both sufficiently low to trigger lysis and sufficiently high to stabilize cells, or that another stabilizing factor such as Ca^{2+} is present [46]. In either case, the round cell morphology is consistent with the outer membrane remaining intact inside the vacuole [39]. We therefore revisited the design of the SLD to include a protein capable of independently lysing the outer membrane.

Bacteriocin release protein (BRP) from *E. coli* permeabilizes the outer membrane by activating phospholipase A [47]. To minimize the toxic effects of expressing wild-type BRP in *E. coli*, we used a modified BRP bearing an unstable N-terminal murein lipoprotein signal peptide and additional detoxifying mutations [48]. We monitored the release of periplasmic alkaline phosphatase (PhoA) into the supernatant as a function of BRP expression to validate its function. PhoA activity increased with increasing BRP expression (Figure 1.6), confirming BRP activity. We then incorporated BRP into the first, promoterless operon of the original SLD and confirmed maintenance of lysis activity *in vitro* (Figure 1.4A and 1.4B), and subsequently observed successful delivery of payload to the vacuole *in vivo* (Figure 1.2C).

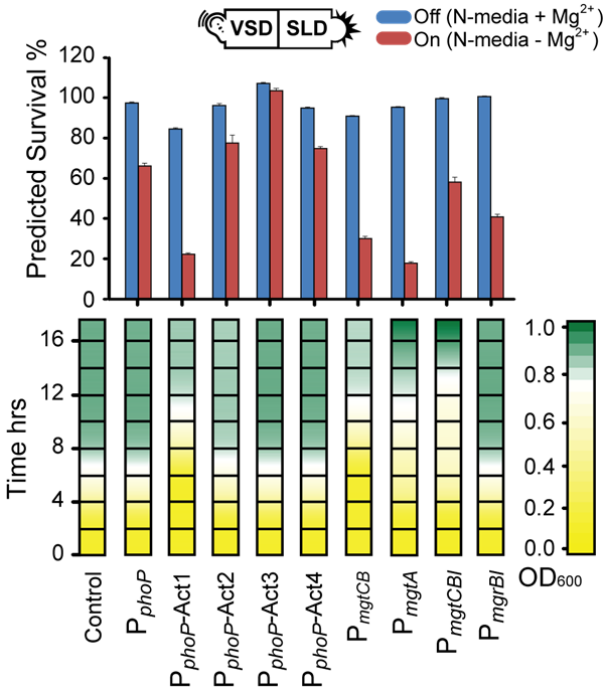

Figure 1.5 Characterization of the VSD-SLD combinations
The degree of lysis from the VSD and SLD combinations in both the Off and On state were predicted, with error bars calculated from the standard deviation of the relative transcription measurements of the VSD. Growth curves of devices in LB + Mg^{2+} were also measured; the mean of 4 replicates is illustrated. Error bars indicate the standard deviation of 3 biological replicates.

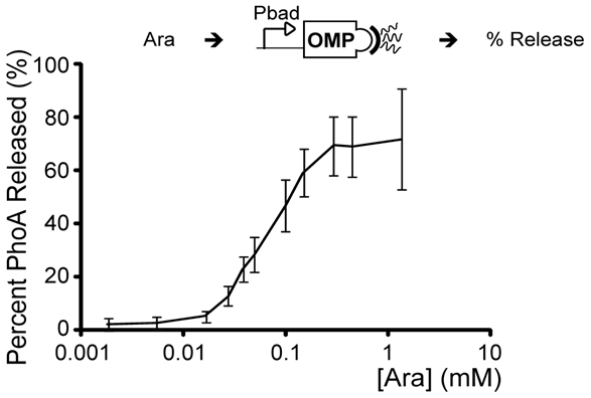

Figure 1.6 Confirmation of BRP function
Assessment of *brp* activity at different expression levels, monitored by release of the periplasmic protein, PhoA. Error bars are the standard deviation of 4 biological replicates.

1.2.4.2 Complete system integration *in vivo*

We constructed complete payload delivery systems by adding VSD-driven variants of the VLD into cells possessing the ID and VSD-driven SLD and assayed them for delivery efficiency and cytotoxicity (Figure 1.7). PFO and PLC with N-terminal degrons had the highest delivery efficiency, delivering the payload to 15 % of invaded target cells. However, all device variants had similarly low levels of cytotoxicity, irrespective of the presence of an N-terminal degron, suggesting that the amount of vacuole lysing proteins delivered to the cytosol was below toxic levels. Further, the majority of invaded mammalian cells internalized 1-3 bacteria but contained unlysed vacuoles filled with GFP (data not shown), suggesting insufficient VLD activity. Based on these observations, we sought to further improve payload delivery efficiency by decoupling expression of the VLD proteins from the VSD, thus providing time for the proteins to build to higher levels before self-lysis. Figure 1.8 illustrates that use of a constitutive promoter to drive the VLD increased the payload delivery efficiency from 15 % to 50 % without any increase in cytotoxicity.

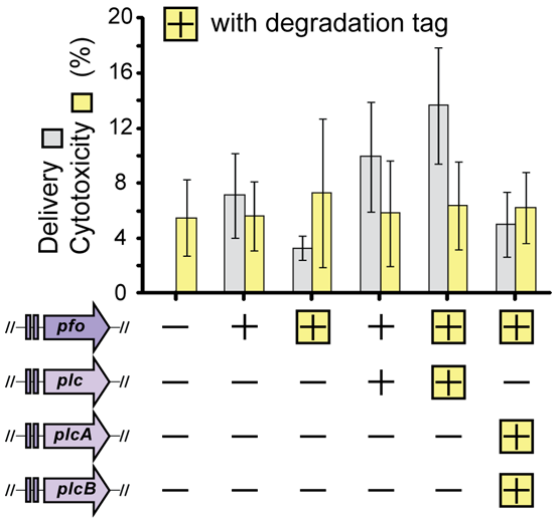

Figure 1.7 Characterization of the vacuole lysis devices
Fluorescent protein payloads were delivered to U373 MG cells *in vivo*, and the efficiency of delivery and cytotoxicity was measured for each VLD variant. (+) indicates the device is installed, Boxed (+) indicates the device with degradation tag is installed, (-) indicates the device is not installed. Error bars indicate the standard deviation of 3 biological replicates. Error bars indicate the standard deviation of 3 biological replicates.

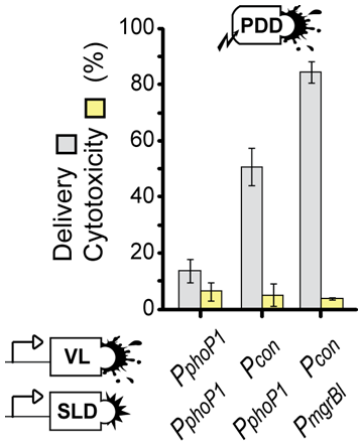

Figure 1.8 Improvements of the payload delivery devices
Payload delivery was evaluated using different promoters to drive the VLD and SLD. Error bars indicate the standard deviation of 3 biological replicates.

1.2.4.3 Optimization of the complete system by predicting the output of connected devices

As a final optimization step, we revisited the VSD module, evaluating four derivatives of the P_{phoP} promoter bearing transcriptional amplifiers (Figure 1.1A) and four additional known PhoPQ responsive promoters (P_{mgtCB}, P_{mgtA}, P_{mgtCBI}, and P_{mgrBI}). We expected that successful VSD-VLD combinations could be predicted by measuring the transcription output of the VSD variants (Figure 1.3).

To do this, the relative transcription of P_{BAD} was measured using the method described in the methods section (1.4.3), except that the N-medium used for resuspension was supplemented with 0-1.33 mM arabinose. This allowed us to generate a transfer curve between arabinose concentration and relative transcription (Figure 1.9). When assaying the SLD for lysis activity, identical arabinose concentrations were employed and mapped one-to-one to the mean measured relative transcription for that arabinose value. To predict the percent survival of each VSD driving expression of the SLD, the measured relative transcription of the VSD was mapped to the corresponding measured percent lysis in the presence or absence of Mg^{2+}. A best fit curve was then generated from this data (Figure 1.10) and used to predict the theoretical performance of each of the VSD-SLD combinations (Figure 1.5).

We performed a preliminary validation of these predictions by measuring the growth rate of cells bearing each device combination (Figure 1.5). The two VSDs predicted to cause the highest basal self-lysis activity, P_{mgtCB} and P_{phoP}-act1, showed clear growth defects. P_{phoP}-act2, P_{phoP}-act3, P_{phoP}-act4, P_{mgrBI}, and P_{phoP} driving the SLD grew comparably to the control, consistent with their predicted low basal self-lysis activity. The device combinations using P_{mgtA} and P_{mgtCBI} showed an unexpected phenotype. Their slow growth eventually exceeded the cell density of a device-free control. They were excluded from further consideration. These results indicate that simple transcription measurements can be useful in predicting potentially successful device combinations; however, additional work is needed to

fine-tune the approach. The stability and high predicted activity of P_{mgrBl} VSD module was further tested in the complete system. We observed that replacement of the P_{phoP} VSD module with P_{mgrBl} VSD module significantly improved payload delivery to over 80 % (Figure 1.8). This increase in efficiency was consistent with what we expected from the prediction.

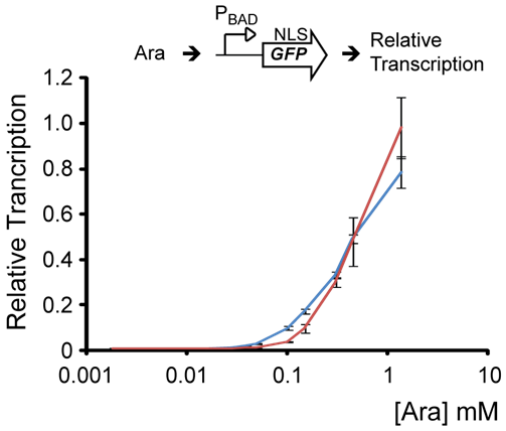

Figure 1.9 Mapping arabinose concentration to relative transcription
In order to map arabinose concentration to relative transcription, a transfer curve was generated by measuring the relative transcription of P_{BAD} both with (N-medium + Mg^{2+}; blue) and without (N-medium - Mg^{2+}; red) Mg^{2+}. Measurements were taken using *E. coli* in 0-1.33 mM arabinose. Error bars are the standard deviation of 4 replicates.

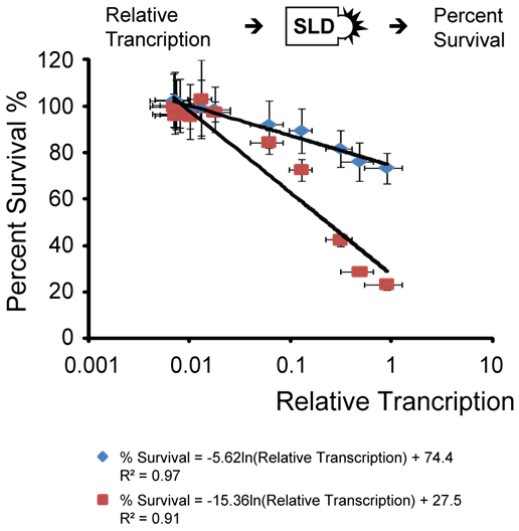

Figure 1.10 Mapping relative transcription to percent lysis
To map relative transcription to lysis efficiency, a curve of best fit was generated for measured relative transcription versus percent survival. *E. coli* bearing a P_{BAD} driven SLD(λ) was induced with 0-1.33 mM arabinose, which was mapped to relative transcription. Percent survival, as compared to *E. coli* with no plasmid, is shown in N-medium + Mg^{2+} (blue) and N-medium - Mg^{2+} (red). Vertical error bars are the standard deviation of 4 replicates, while horizontal error bars reflect the standard deviation of the measured relative transcription in part A. The equations and R squared values for the lines of best fit are displayed.

1.3 Discussion

The bacterial delivery system developed here provides a mechanism for efficient delivery of payloads to mammalian cells. By engineering an active lysis system, rather than relying on passive lysis through slow growth in the vacuole, the payload delivery device avoids complications arising from using DAP auxotrophs. This expands the repertoire of tools available for development of probiotic or therapeutic applications. We envision that the delivery system itself will become a high level module. It can be incorporated into the design of more complex systems, such as a therapeutic bacterium delivering cancer-cell specific microRNA [7], or a mechanism for genetically or biochemically manipulating otherwise intractable eukaryotes as described in Chapter 3.

We successfully applied a modular design framework to engineering *E. coli* to deliver macromolecules to mammalian cells. This entailed partitioning the system into five modules: payload generation, invasion, vacuole microenvironment sensing, bacterial self-lysis, and vacuole lysis. In doing so, we sought to explore the utility of modular design for engineering complex biological systems. In particular, this meant assessing the validity of two critical assumptions: that modules of biological functionality can be independently fabricated and tested, and that modules can be predictably combined and connected to generate higher order behavior.

We chose to use transcriptional boundaries to delineate component devices; each primitive device either stimulates transcription or transduces transcription into a biochemical event. Composition of devices then couples transcription and/or biochemical events together to evoke more complex behavior. In this framework, the invasion and payload generation devices can be conceived of as constitutive transcription devices joined to basic functional devices. The use of transcriptional interface greatly facilitated independent testing of basic modules, since output transcription can be readily measured and input transcription can be readily controlled.

While testing the modules, however, we encountered two important limitations. First, we were unable to test the vacuole lysis device in the absence of other devices. Dependence on other devices for testing requires that two unknowns be considered in parallel: the function of the module and the connection of the module to its dependencies. Second, our independent test of self-lysis turned out to be an inadequate proxy for the final *in vivo* context of the module. Although the original design lysed well under *in vitro* assay conditions, we overlooked the importance of the reduced ionic strength inside a vacuole. The ability of our *in vivo* assay to distinguish between no lysis and partial lysis helped us to isolate the problem. Swapping in a module containing BRP rapidly resolved the issue. This, however, points to a potentially cumbersome problem. With a less detailed assay, we might have believed that the failure lay in the connection between the vacuole sensing device and the self-lysis device, rather than in the self-lysis device itself. Changes in assay conditions must therefore also be considered as a potential failure mode.

Most module combinations also behaved as expected. In particular, the payload generation and invasion devices readily combined with the final vacuole sensing, self-lysis, and vacuole lysis devices to create a functioning system. While we did encounter a few failures, they served to illustrate the strength of a modular design

approach. First, the unexpected behavior of a few constructs *in vitro* highlights how incomplete information can cause failures. We did not initially expect any expression level of the self-lysis device to cause slow but strong growth, regardless of the growth conditions; only an *ex post facto* search revealed an explanation for such behavior. Although we suspect that this type of failure is rare, it can be readily isolated to a junction between two modules and thus presents only a minor design obstacle. Second, our initial connection between the vacuole sensing device and vacuole lysis device caused inefficient payload delivery. We had presumed, without evidence, that constitutive expression of the vacuole lysis device would prove toxic to the mammalian cells, and therefore triggered expression of the vacuole lysis device only after sensing the vacuole. After observing low efficiency with this connectivity, however, we recognized the assumption we had made and chose to decouple the vacuole lysis device from the vacuole sensing device. Because of the modular design of the system, this required only the exchange of a single promoter, which proved to greatly improve the system efficiency. In terms of design considerations, it may have been the case that transcription of the vacuole lysis device was in fact sufficient to cause vacuole lysis if allowed to act for several hours, but not when prematurely interrupted by self-lysis. It is not difficult to imagine other scenarios where the duration of transcription or the speed at which transcription changes from one level to another is important to the behavior of the system, and our simple analysis provides no framework for considering such timing requirements. Extension of the simple relative transcription measurement approach may be needed to enable applications with complex timing.

1.3.1 Qualitative behavior of devices

It is clear that we were able to describe and predict a device hierarchy of abstract cellular functions in a qualitative way. However, our success in making quantitative predictions about how to combine modules leading to matched impedance was minimal. There are currently no formally-described and experimentally-verified methods that reliably predict the quantitative behavior of devices on the basis of parameters encapsulated onto specific DNA sequences. In our study, we examined one leading contender for such a method, that of RPU. Although this analysis did give us some qualitative hints about how to improve our system, there was not a strong quantitative correlation between the predicted expression levels and the observed behavior.

Part of our difficulty came from trying to apply the RPU concept to a design problem with exceptions that were not addressed in the original description of the RPU concept. These included the fact that we needed to compare gene expression levels across different media compositions rather than amongst data points collected all in one environmental state. Additionally, the behaviors themselves that we were engineering, particularly self-lysis, intrinsically affect the viability and growth rate of the bacteria. This led to an unclear means of synchronizing measurements and correlating them to OD data. This was further complicated by the fact that measuring the density of the bacteria to quantify self-lysis, appeared to be affected by the conditions the cells were grown in. In particular, Mg^{2+} concentrations influenced how the well the bacteria lysed. Additionally, several of the constructs exhibited unusual growth behavior indicating the presence of stress and load on the cell that further

complicated the measurements. Ultimately, our results do not refute the assumptions of the RPU concept, but they do point to clear limitations to this simple theory of expression modeling. We encountered numerous edge cases that made the validity of such analyses impossible without ‘hacks’ to the original idea, which we cannot currently justify with any formal theory. It is apparent from these studies that robust models of gene expression that deal with the edge cases of altered media, the effects of cellular stress and load, and the means of experimentally separating measurement effects from those of the underlying chemical system must be developed.

Our current ability to design systems on this level of complexity is primarily limited by two theoretical barriers: we have not formulated complete formal descriptions of cellular behavior that fully connect basic physicochemical concepts to higher-level concepts. We are accustomed to dealing with these missing layers through experience, intuition, and generally-believed rules-of-thumb. The result of this is that we contain lower-level indefinite abstractions within our understanding of our devices that does not enable us to make concrete quantitative predictions about the behavior of variants of those devices. In addition, we do not have theoretical models of cellular stress and load sufficient to describe the linkage between arbitrarily chosen genetic features and the effects on the growth rate, expression levels, and viability of cells produced by combining those features. Our work here presents a clear demonstration of the limitations caused by these two gaps in formal mapping between underlying physicochemical theory and higher level abstractions. However, the observation that we can construct a system as complex as payload delivery employing only qualitative descriptions of cellular function suggests that these are secondary considerations. Of primary importance is a design strategy where the sequential evaluation of each module and module composition reduces the number of factors under consideration at each step and isolates unexpected behaviors. Application of such a strategy enables *a priori* specification of the molecular functions required to achieve a desired behavior and facilities subsequent troubleshooting and optimization.

1.4 Material and Methods

1.4.1 Plasmids and Strains

The genetic constructs used in this study were constructed using BglBrick standard assembly [50], a variation on BioBrick standard assembly using the *Bgl*II and *Bam*HI restriction enzymes. To facility part assembly, methylating strains of *E. coli* were employed [51]. All experiments were performed with *E. coli* strains MG1655, MC1061, and derivatives thereof (Table 1.4). Sequences of DNAs used to fabricate composite devices are available in the MIT Registry of Standard Biological Parts [52]. The complete composition of devices is available in Appendix (Table 1.2).

1.4.2 Growth medium and condition

E. coli were grown in Luria Broth (LB) medium for routine molecular biology protocols. Cultures for assay experiments were grown in LB, LB supplemented with 30 mM $MgSO_4$ (LB + Mg^{2+}), N-minimal medium supplemented with 0.1 % casamino acids, 38 mM glycerol (N-medium) [53], and 30 mM or 0 mM $MgSO_4$ (N-medium +/- Mg^{2+}), or Terrific Broth (TB) supplemented with 30 mM of $MgSO_4$ (TB + Mg^{2+}). Cultures were incubated at 37 °C with 700 rpm shaking in a Multitron Standard orbital plate shaker (Infors-HT, Bottmingen, Switzerland).

1.4.3 Relative transcription determination

Relative transcription was determined essentially as described previously [23], except that cells were assayed under specific, non-logarithmic growth conditions. Briefly, samples of stationary phase *E. coli* cells grown in LB + Mg^{2+} bearing a plasmid with either a constitutive standard reference promoter (P_{REF}) or a test promoter (P_{TEST}) driving expression of green fluorescent protein were subcultured 1:100 into fresh LB + Mg^{2+} and grown until reaching an OD_{600} of 0.5. They were subsequently washed twice with N-medium +/- Mg^{2+} and re-suspended in the same medium. They were then incubated at 37 °C for 6.5 hrs, and the OD_{600} (OD) and fluorescence intensity (F - excitation 501 nm, emission 511 nm) measured with a fluorescent plate reader. Relative transcription was then calculated as $\{F(P_{TEST})/OD(P_{TEST})\}/\{F(P_{REF})/OD(P_{REF})\}$.

1.4.4 Assay for self-lysis activity

E. coli bearing an arabinose-inducible promoter (P_{BAD}) driven SLD were grown to stationary phase in LB + Mg^{2+}. They were then diluted 1:100 into fresh LB + Mg^{2+} medium and grown to an OD_{600} of 0.5. Bacteria were collected by centrifugation, washed twice with N-medium +/- Mg^{2+} and resuspended to an OD_{600} of 0.5 in N-medium +/- Mg^{2+} containing 0-1.33 mM arabinose. They were incubated at 37 °C for 6.5 hrs, and the OD_{600} measured with a plate reader. Percent survival was calculated as sample OD_{600} divided by control OD_{600} (*E. coli* without SLD), and arabinose concentration was mapped to relative transcription.

1.4.5 PhoA release assay

E. coli bearing a constitutive PhoA expression plasmid with or without a P_{BAD}-*brp* expression plasmid was grown to stationary phase in LB. Cells were diluted 1:100 into fresh LB + 0-1.33 mM arabinose, and incubated at 37 °C for 6.5 hrs. After incubation, cells were harvested by centrifugation, and the supernatant was assayed for PhoA activity essentially as described previously [54]. Briefly, 25 µL of supernatant was transferred into a total of 250 µL containing 0.001% SDS, 10 µg/ml 4-nitrophenyl phosphate, and 80 mM tris (pH 8). Samples were incubated for 2 hours at 37 °C, then transferred to a Corning flat-bottom 96 well microplate and the absorbance at 420 nm was measured.

1.4.6 Growth curve determination

E. coli bearing VSDs driving a SLD or a plasmid-less control were grown to stationary phase in LB + Mg^{2+}. These were subcultured 1:100 into fresh LB + Mg^{2+}, and a 200 µL aliquot was transferred to a Corning flat-bottom 96 well microplate. The plate was incubated at 37 °C, and the OD_{600} measured every five minutes.

1.4.7 Microscopy of devices

A monolayer of HeLa or U373 MG cells was prepared 24 hours prior to experimentation on an 8-well chambered slide (LabTech) in growth medium (DMEM supplemented with 10 % fetal bovine serum (FBS) for HeLa and DMEM supplemented with 1 % non-essential amino acids (NEAA), 1 mM sodium pyruvate, and 10 % FBS for U373 MG) with penicillin and streptomycin antibiotics. The medium was replaced with fresh medium without antibiotics, and stationary phase bacterial culture (grown in TB + Mg^{2+}) was added to each well. For experiments without a VLD, 1 µL of bacteria and HeLa were used, resulting in an average of 20-80 internalized bacteria per mammalian cell, while for experiments with a VLD, 0.5 µL of bacteria and U373 MG were used, resulting in an average of 1-3 internalized bacteria per mammalian cell. After 80 minutes of incubation at 37 °C, cells were washed twice into growth medium with 100 µg/mL gentamicin, and the slides incubated for a further 3.5 hours before the examination by microscopy. Images were taken with Zeiss Axiobserver D1 or Zeiss Axiovision Z1 inverted microscope equipped with Hamamatsu 9100-13 EMCCD camera. For complete PDD, the delivery efficiency was quantified as the number cells with a green nucleus divided by the number of cells bearing internalized bacteria and/or a green nucleus. To determine cytotoxicity after the 3.5 hour incubation, each well was incubated with PBS containing a final concentration of 4 µM of ethidium homodimer-1 (EthD-1) (Life Technologies) and 2 µM of Hoechst 33342 (VWR) for 10 min at 37 °C. EthD-1 stains the nucleus of membrane permeabilized (dead) cells and Hoechst stains the nucleus of all cells. Cytotoxicity was calculated as the number of EthD-1 stained cells divided by the number of cells bearing internalized bacteria and/or a green nucleus.

1.4.8 Biosafety and biosecurity considerations

All experiments followed the guidelines of the Office of Environment, Health,

and Safety (EH&S) at UC Berkeley. Since many of the strains used in these studies involved virulence factors from risk group 2 (RG2) organisms, these materials are regarded as RG2 and our work operated under biosafety level 2 protocols. High affinity iron transport mutants (Δ*tonB*) were employed to mitigate any risks to researchers or the environment posed by these organisms. To mitigate potential dual-use of these materials, only the RG1 parts are fully described at base-level precision. Full sequences including RG2 components and physical DNAs are available upon request from researchers presenting evidence of institutional approval.

1.5 Table

Table 1.1 Plasmids used in experiments

Figure	Label	Plasmid
1.2A	Payload Device	Bjh2313-BBa_J72117
1.2B	Payload Device	Bjh2313-BBa_J72117
	VSD(P_{phoP}) driven SLD(λ)	Bjh1239-BBa_J72118
1.2C	Payload Device	Bjh2313-BBa_J72117
	VSD(P_{phoP}) driving SLD(λ) with BRP	Bjh1874-BBa_J72118
1.2D	Payload Device	Bjh2313-BBa_J72117
	PDD with P_{CON} driving VLD(degradation tagged *pfo*/*plc*) and VSD(P_{mgrBl}) driving a SLD(λ) with BRP	Bjh2399-BBa_J72118
1.3	P_{REF} driven GFP	Bjh2302-BBa_J72118
	VSD(P_{mgtCB}) driven GFP	Bjh2389-BBa_J72118
	VSD(P_{phoP}) driven GFP	Bjh2297-BBa_J72118
	VSD(P_{mgtCBl}) driven GFP	Bjh2387-BBa_J72118
	VSD(P_{mgrBl}) driven GFP	Bjh2386-BBa_J72118
	VSD(P_{mgtA}) driven GFP	Bjh2388-BBa_J72118
	VSD(P_{phoP}-Act1) driven GFP	Bjh2299-BBa_J72118
	VSD(P_{phoP}-Act2) driven GFP	Bjh2325-BBa_J72118
	VSD(P_{phoP}-Act3) driven GFP	Bjh2300-BBa_J72118
	VSD(P_{phoP}-Act4) driven GFP	Bjh2298-BBa_J72118
1.4	P_{BAD} driven SLD(λ)	Bxa160-BBa_J72118
	P_{BAD} driven SLD(T4)	Bjh1998-BBa_J72118
1.5	VSD(P_{mgtCB}) driven SLD(λ)	Bjh1236-BBa_J72118
	VSD(P_{phoP}) driven SLD(λ)	Bjh1239-BBa_J72118

	VSD(P_{mgtCBl}) driven SLD(λ)	Bjh1242-BBa_J72118
	VSD(P_{mgrBl}) driven SLD(λ)	Bjh2369-BBa_J72118
	VSD(P_{mgtA}) driven SLD(λ)	Bjh2370-BBa_J72118
	VSD(P_{phoP}-Act1) driven SLD(λ)	Bjh2372-BBa_J72118
	VSD(P_{phoP}-Act2) driven SLD(λ)	Bjh2374-BBa_J72118
	VSD(P_{phoP}-Act3) driven SLD(λ)	Bjh2373-BBa_J72118
	VSD(P_{phoP}-Act4) driven SLD(λ)	Bjh2371-BBa_J72118
1.6	P_{BAD}-*brp* expression plasmid	Bjh2109-BBa_J72118
	constitutive PhoA expression plasmid	Bjh2143c12-BBa_J72117
1.7	VSD(P_{phoP}) driving SLD(λ) with BRP	Bjh1874-BBa_J72118
	VSD(P_{phoP}) driving SLD(λ) with BRP and VLD(*pfo*)	Bjh1865-BBa_J72118
	VSD(P_{phoP}) driving SLD(λ) with BRP and VLD(degradation tagged *pfo*)	Bjh1866-BBa_J72118
	VSD(P_{phoP}) driving SLD(λ) with BRP and VLD(*pfo*, *plc*)	Bjh1864-BBa_J72118
	VSD(P_{phoP}) driving SLD(λ) with BRP and VLD(degradation tagged *pfo* and *plc*)	Bjh1872-BBa_J72118
	VSD(P_{phoP}) driving SLD(λ) with BRP and VLD(degradation tagged *pfo*, *plcA*, and *plcB*)	Bjh2268-BBa_J72118
1.8	PDD with VSD(P_{phoP}) driving both VLD and SLD	Bjh1872-BBa_J72118
	PDD with P_{CON} driving VLD(degradation tagged *pfo*/*plc*) and VSD(P_{phoP}) driving SLD(λ) with BRP	Bjh2348-BBa_J72118
	PDD with P_{CON} driving VLD(degradation tagged *pfo*/*plc*) and VSD(P_{mgrBl}) driving a SLD(λ) with BRP	Bjh2399-BBa_J72118
1.9	P_{REF} driven GFP	Bjh2302-BBa_J72118
	P_{BAD} driven GFP	Bjh2366-BBa_J72118
1.10	P_{REF} driven GFP	Bjh2302-BBa_J72118
	P_{BAD} driven GFP	Bjh2366-BBa_J72118
	P_{BAD} driven SLD(λ)	Bxa160-BBa_J72118

Table 1.2 Strains used in experiments

Figure	Strain*
1.3, 1.4, 1.5, 1.9, 1.10	MC1061
1.2A, 1.2B, 1.2C	JH-3-E9 (MG1655 attP21::P_{flu}-*inv*)
1.2D,1.7, 1.8	JH-4-C3 (MG1655 Δ*tonB* attP21::P_{flu}-*inv*)
1.6	JH-5-19 (MC1061 Δ*tonB* attP21::P_{flu}-*inv*)

* Strain modifications were made using standard techniques [55, 56,57].

Chapter 2

Payload Secretion Device

2.1 Introduction

The payload delivery device developed in Chapter 1 is a useful strategy for delivering proteins to target mammalian cells. However, it harbors some intrinsic limitations. First, unwanted bacterial components such as proteins, lipids, and nucleotides are co-delivered along with the payload. Second, the amount of payload per bacterium is limited due to stability or toxicity of payload in the cytoplasm of the bacterium. Finally, the entire payload is delivered in a single burst, and the rate of release cannot be controlled. These limitations would be irrelevant for some applications such as delivering toxins to cancer cells, because the target cell will be going through apoptosis eventually. However, they may become more significant for applications that require greater control over payload delivery such as delivering therapeutics to target cells.

To address this, we developed a new strategy of payload delivery where *E. coli* is programmed to escape from the vacuole after invasion of target mammalian cells and continuously secrete the payload inside the cytoplasm of the target mammalian cell. Once the payload delivery is completed, *E. coli* are removed by autophagy (Figure 2.1). Autophagy is a cellular process that recycles cellular components, including organelles or intracellular bacteria, through lysosomal machinery in response to nutrient starvation, organelle damage, or microbial infection (58 and references therein). We can utilize this process to remove our *E. coli*., leaving the target cell minimally affected [59].

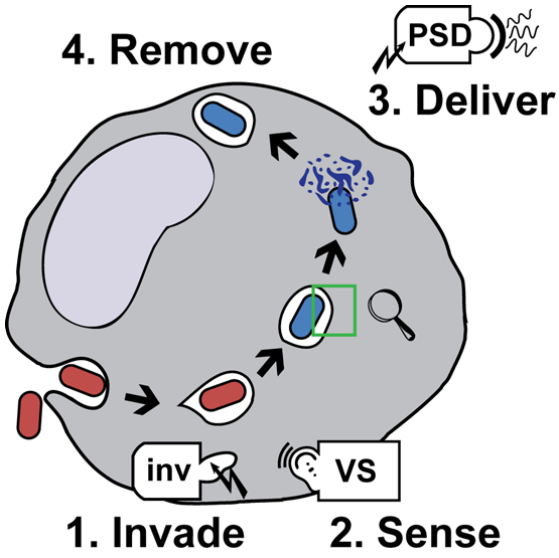

Figure 2.1 The strategy of the payload secretion device
The fundamental flow of operation is to invade, sense, deliver, and removal. The invasion device allows *E. coli* to enter the target cell. The vacuole sensor device activates the payload secretion devices, which delivers payloads to the cytoplasm of the target cell. Once the delivery is completed, *E. coli* is removed by autophagy.

Alternative gene therapy (AGT) is a mode of delivery that is most similar to the payload secretion [60]. It has shown positive results for various disease models including liver cancer, refractory cancer, mammary carcinoma, adenocarcinoma, ischemia, and solid tumor [61, 62, 63, 64, 65, 66, 67]. In this strategy, a bacterium resides in the extracellular space of the target tissue and delivers payloads in a manner dependent on small molecule inducers. Payload delivery can be stopped when needed, and the bacterium can be removed by means of antibiotics. However, payloads produced by the bacterium may diffuse away from the target cells, and it would be difficult to deliver similar doses of payloads to each target cell. We anticipate that the payload secretion device may provide a new delivery strategy that addresses these limitations as well.

In Chapter 1, we demonstrated that we can efficiently and systematically engineer a complex biological system. In this chapter, we attempted to further assess the validity of abstraction and modularity when engineering the payload secretion device. Abstraction and modularity are one of the engineering principles that enable reuse of modular devices for another purpose that is different from the original. Equipped with the characterization of devices obtained in Chapter 1, we were able to rationally rearrange genetic elements and obtain new function. We simply rearranged the existing devices obtained from Chapter 1.

2.2 Results

2.2.1 Assembly and troubleshooting of the payload secretion device

Similar to the payload delivery device in Chapter 1, the secretion device had to transport payload across four physical barriers: the bacterial inner membrane, the peptidoglycan layer, the outer membrane, and the mammalian vacuole membrane. Here, however, transport could not utilize self-lysis of bacterium. Thus we designed a construct that leaves the inner membrane and peptidoglycan layer intact while outer membrane and vacuole membrane are permeabilized. The vacuole lysis device is targeted to periplasm by the sec transport pathway [68], and reaches the vacuole membrane through permeabilized outer membrane. In order to transport the payload device to periplasm, we utilized the twin arginine translocation (TAT) pathway [69], since fluorescent proteins are unable to fold in periplasm after they are secreted by the sec transport pathway [70]. The signal peptide of TorA was attached at the N-terminus of both GFP-NLS and RFP [69].

When the vacuole sensor device was activated, our *E. coli* were designed to release the pre-loaded payload device and the newly synthesized vacuole lysis device from the periplasm to vacuolar space. After the vacuole membrane was degraded, *E. coli* was to reside in the cytoplasm of target cells, and continuously synthesize and secrete the payloads. Therefore, the payload was placed under a constitutive promoter, such that the payload was pre-loaded in periplasm before bacterium was internalized by the invasion device (Figure 2.2A). The BRP and the vacuole lysis device were under the control of the vacuole sensor device. When we tested this *in vivo*, however, the payload was not released from the bacterium (Figure 2.2B).

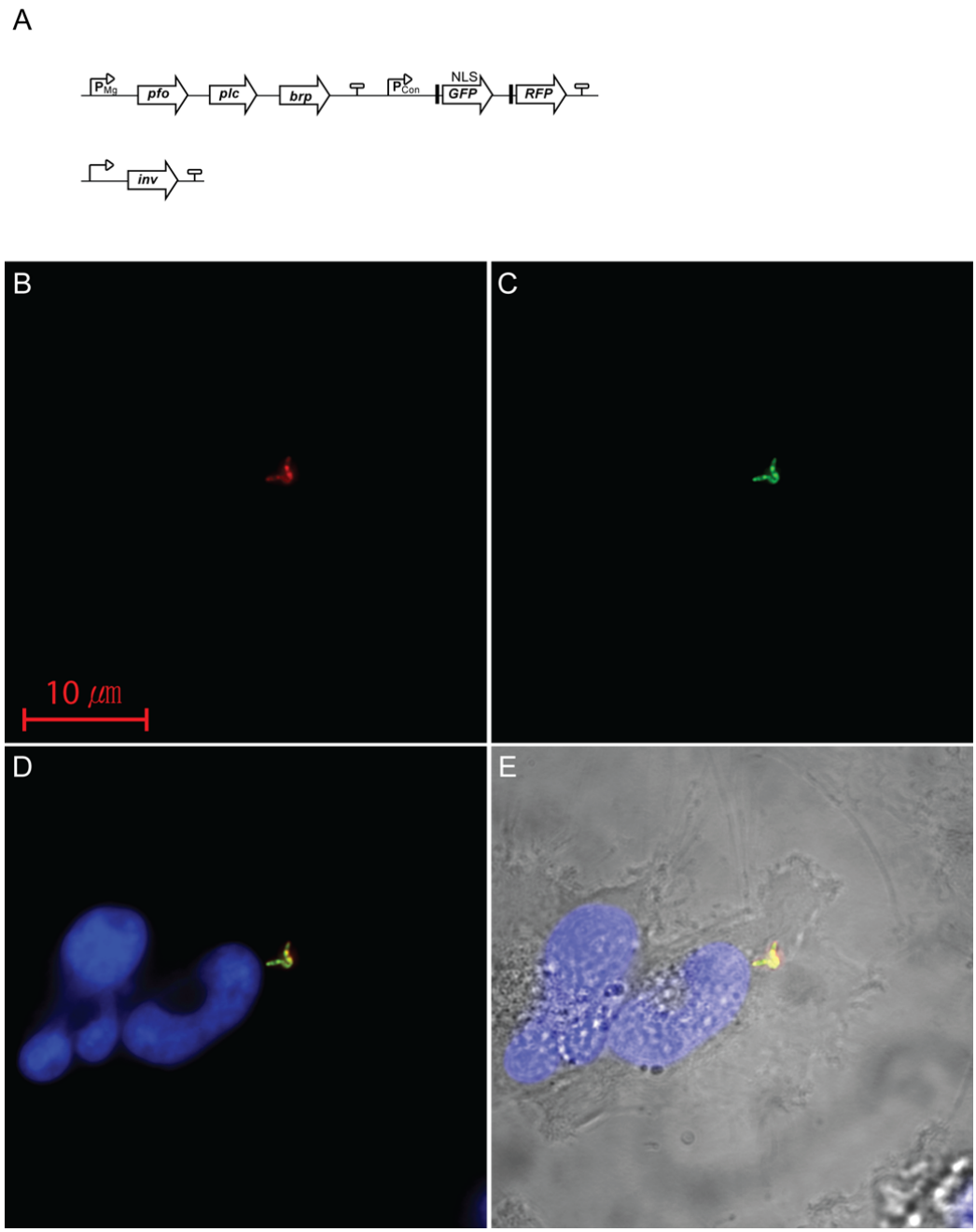

Figure 2.2 Payload was not secreted by TAT pathway

The payloads were targeted to periplasm by TAT pathway. In a successful device, the payload would be released from the outer membrane-permeabilized bacteria upon entry into mammalian cells. However, this was not observed.

A. Device composition

B. RFP was targeted to periplasm, but not released even after outer membrane was permeabilized by BRP.

C. Periplasm targeted GFP-NLS also was not released.

D. Merge: RFP, GFP-NLS, and blue stained nucleus

E. Merge: RFP, GFP-NLS, nucleus, and bright field

In order to solve this problem and release free GFP-NLS and RFP from bacterium, we decided to permeabilize the bacterial inner and outer membrane, because there exist no other simple and easy options to translocate GFP-NLS and RFP from bacterial cytoplasm to periplasm. Holin dimers embedded on inner membrane allow small proteins to freely pass the inner membrane [71]. To build this, we revisited the architecture of the self-lysis device. The device was subdivided into the peptidoglycan layer degrading device, composed of lysozyme, and the inner membrane permeabilizing device (IMP), composed of promoterless holin and antiholin under a constitutive promoter. Then the IMP and BRP were placed under the vacuole sensor device (Figure 2.3C). When this device was installed in *E. coli* and tested *in vivo*, the payload was successfully released from the intact bacteria filling up the vacuole space (Figure 2.3D). When the vacuole lysis device was added (Figure 2.4A), the GFP-NLS was localized to the nucleus after payload was released to the cytoplasm (Figure 2.4B).

Similar to the optimization methods we used for the payload delivery device, we decoupled the expression of the vacuole lysis device from the vacuole sensing device, thus providing time for the vacuole lysis device to pre-load before self-lysis is activated. Figure 2.5 illustrates that use of a constitutive promoter to drive the VLD increased the payload secretion efficiency from ~5 % to ~55 % without any increase in cytotoxicity. Employing the VSD predicted to have the best activity, P_{mgrBI}, further improved efficiency to over 90 %.

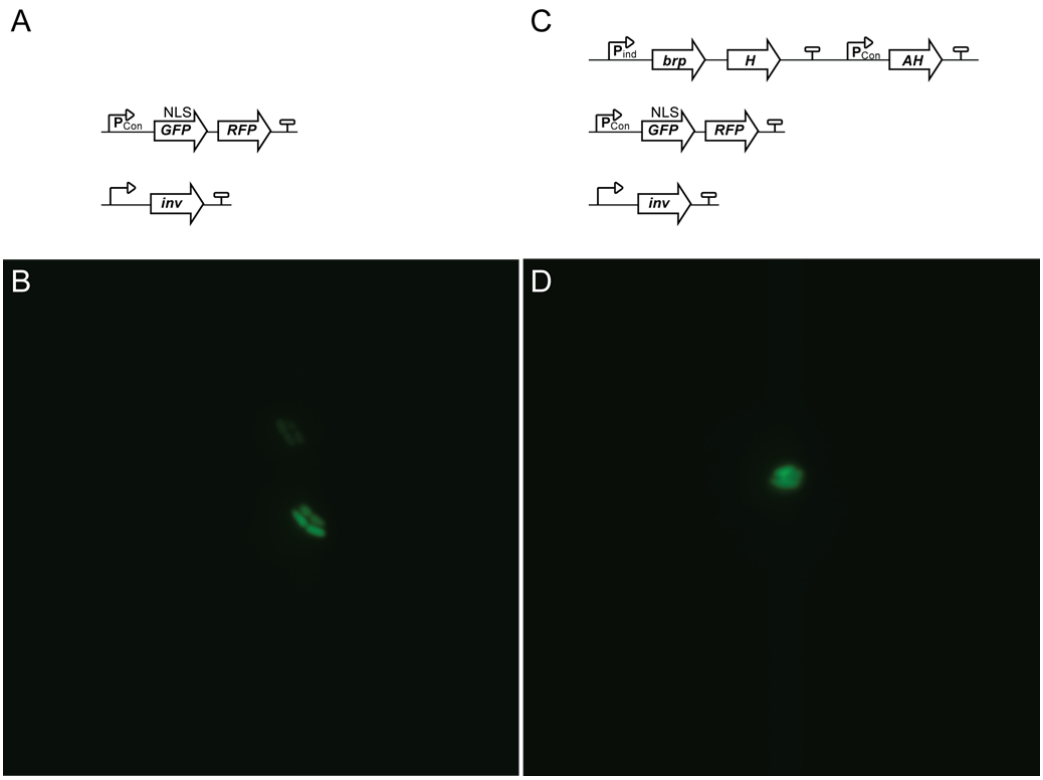

Figure 2.3 Payload was secreted from inner and outer membrane permeabilized bacteria

A. Device composition for B.

B. Bacteria expressing GFP-NLS and RFP in vacuole. Both inner and outer membrane were not permeabilized, and rod shaped bacteriawere observed.

C. Device composition for D. The inner and outer membrane were designed to be permeabilized after they entered the vacuole.

D. The GFP-NLS was distributed in vacuole, which indicated that the GFP was secreted to the vacuole space.

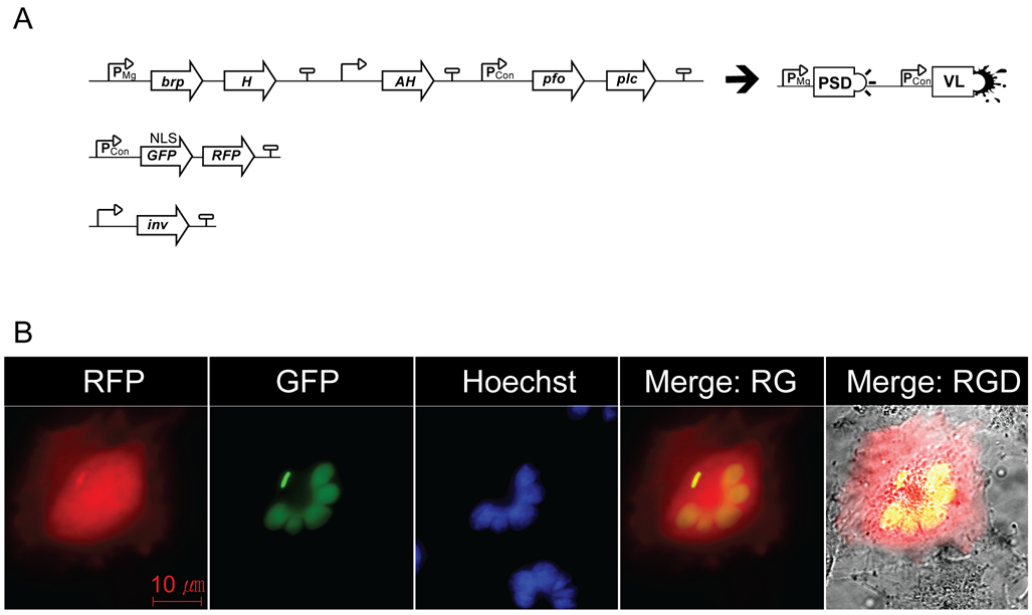

Figure 2.4 Payload secretion device delivered the payload *in vivo*
A. Device composition. The composition of device can be abstracted into the protein secretion and vacuole lysis devices driven by two different promoters.
B. The payload secretion device successfully delivered the payload to the cytoplasm and nucleus of target cell.

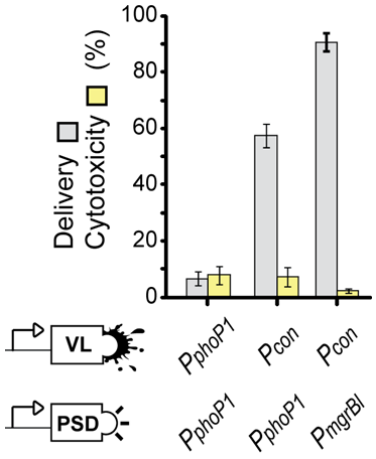

Figure 2.5 Improvements of the payload secretion device
All of the devices have the same architecture except for the promoters for these devices shown. Pre-loading of the VL improved the efficiency. Installation of P_{mgrB} further improved the efficiency. These changes did not affect the cytotoxicity significantly.

2.2.2 Decoupling of vacuole escape and payload delivery

In the payload secretion system described above, the release of the payload was coupled with the vacuole escape. We sought to decouple the timing of the payload delivery and vacuole escape. We then couple the payload delivery with a small molecule inducible promoter such that the payload release is triggered by extracellularly provided small molecules.

In order to make this secretion system compatible with autophagy mediated removal of *E. coli* after delivery is completed, the expression of the vacuole lysis device must be reconsidered. In the previous system, the vacuole lysis device was placed under the constitutive promoter. When *E. coli* are enveloped during autophagy, the vacuole lysis device can allow *E. coli* to escape from the autophagosome, just as it initially escaped from the vacuole. Additionally, although the vacuole lysis device under a constitutive promoter did not cause cytotoxicity within 5 hours of delivery experiment (Figure 2.5), there is a possibility that accumulation over time could damage the host's cytoplasmic membrane when the duration of delivery becomes longer.

Taking all of these into consideration, we further engineered *E. coli* by rearranging the devices. In this design of the payload secretion device, *E. coli* invades mammalian cells, escapes from the vacuole, and initiates payload secretion triggered by an external source of signal. The vacuole lysis device is placed under an orthogonal, inducible promoter, and is pre-loaded in *E. coli* while they are cultured *in vitro* before invasion. They are unable to express the vacuole lysis device thereafter. Thus the bacterium is unable to escape after they are enveloped by the autophagosome.

2.2.2.1 Bacterium escape to cytoplasm

A small molecule inducible promoter, P_{BAD}, was placed before the VLD (Figure 2.6A). The VLD is pre-loaded in the periplasmic space by culturing with the inducer when preparing bacteria for the delivery. BRP is placed under the VSD to release the pre-loaded VLD into the vacuole space, so that bacterium is eventually released to the cytoplasm. The escape of bacterium from the vacuole was monitored by staining acidic vacuoles using LysoTracker™. As a control, bacteria with PSD which were grown without the inducer was compared (Figure 2.6). Bacteria were not able to escape from vacuole and remained in acidic vacuoles. When bacteria were grown with an inducer, bacterium was able to escape to host cytoplasm (Figure 2.7).

We tested another small molecule inducible promoter, P_{RHM}. Although more extensive and comprehensive data for escape efficiency need to be collected, less than 10% of *E. coli* with P_{RHM} driven device have escaped from the vacuole whereas over 90 % of *E. coli* with P_{BAD} driven device were able to escape from the vacuole.

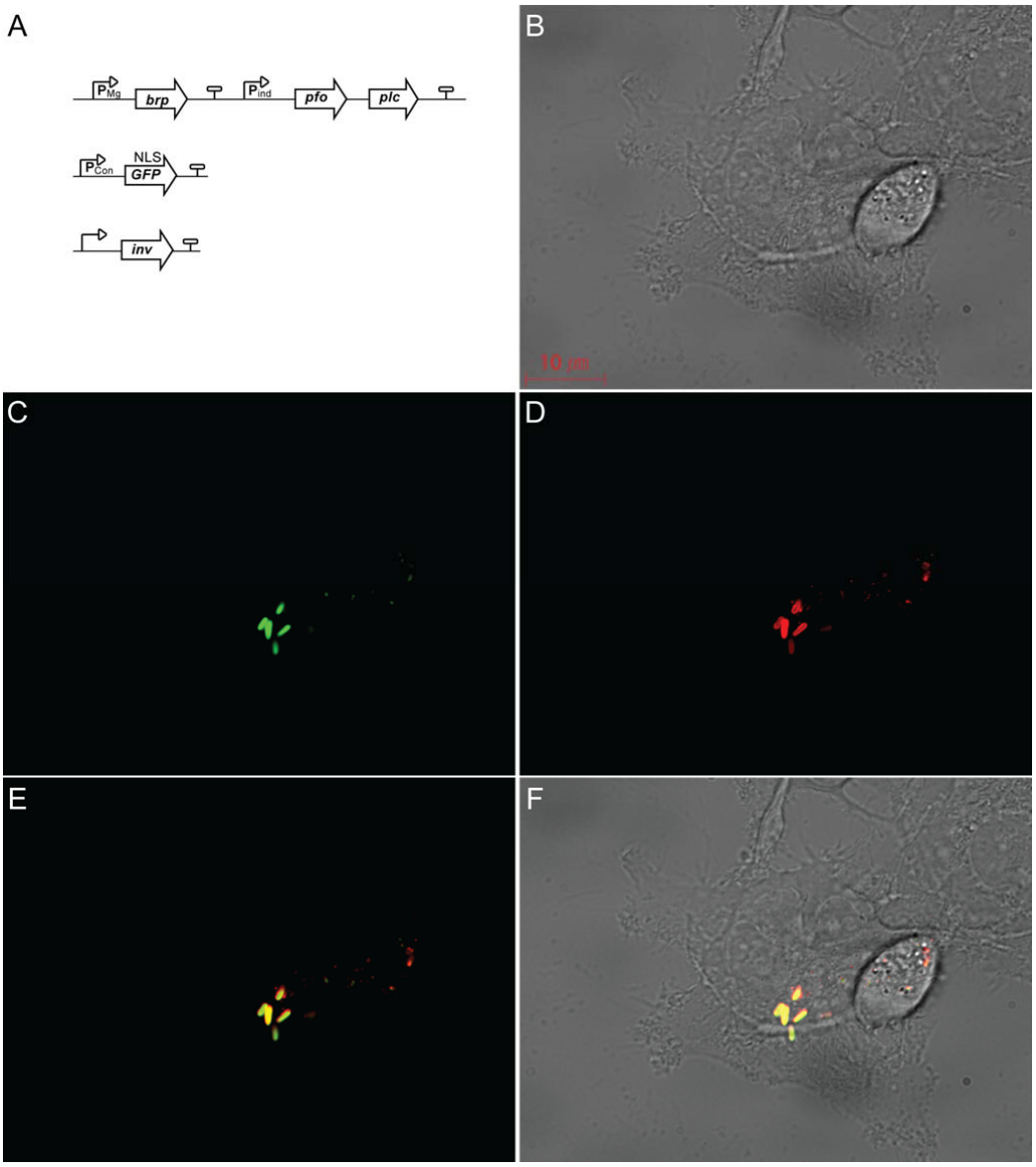

Figure 2.6 *E. coli* remained in phagosome when the vacuole lysis device was not induced

A. Device composition: The vacuole-induced BRP was designed to release the VL, which facilitates the escape of *E. coli* from the vacuole. The expression of the VL was not induced prior to invasion.
B. Bright field image of *M. brevicollis*
C. *E. coli* expressing GFP in vacuole of *M. brevicollis*.
D. *M. brevicollis* vacuole stained with LysoTracker™.
E. Merge: green and red channel. Co-localization of green and red indicated that bacteria did not escape from the vacuole.
F. Merge: green, red, and bright field channel

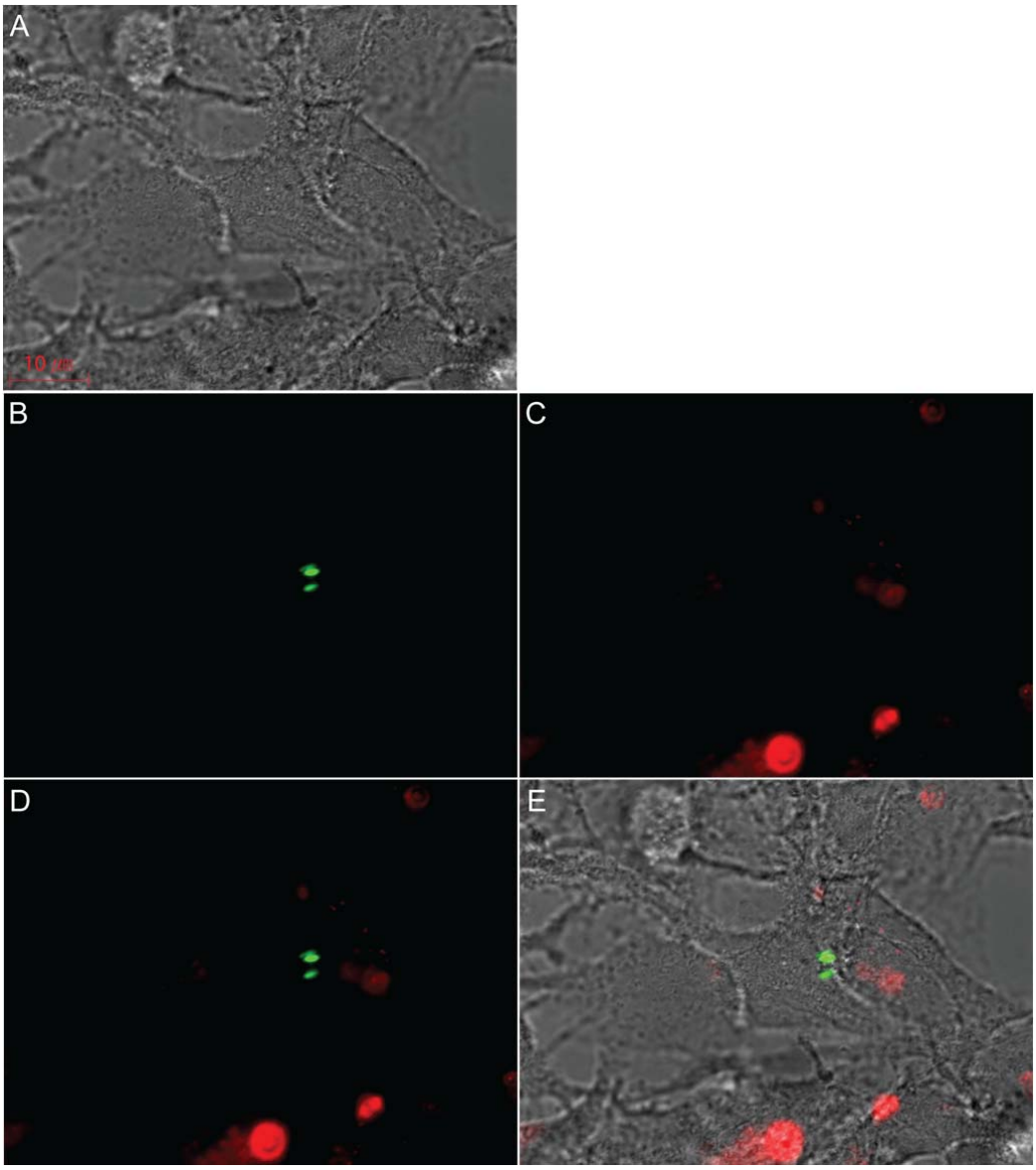

Figure 2.7 *E. coli* escaped from phagosome when the vacuole lysis device was induced

A. Bright field image of *M. brevicollis*

B. *E. coli* expressing GFP. This bactaria contains an identical device composition as the bacteria in Figure 2.6A, but the expression of the VL was induced prior to invasion.

C. The vacuole stained with LysoTracker™.

D. Green and red channel were merged. Bacteria containing vacuole was not stained, which indicated that bacteria escaped from the vacuole.

E. Green, red, and bright field channel were merged.

2.2.2.2 *E. coli* in host cytoplasm respond to small molecules

Validation of metabolic viability of *E. coli* within a mammalian cytoplasm comes from testing whether gene expression can be triggered after they escape from vacuole. Small molecule inducers are supplied in the mammalian growth medium, and trigger gene expression of a visible signal once they reach the *E. coli* dwelling in the cytoplasm.

The success of this experiment faced one fundamental challenge. Even after an extensive, post-invasion wash, it was difficult to remove all extracellular bacteria from the well. Subsequently, bacteria outside of the cell may have become induced and internalized, but perceived as a response from already intracellular bacteria. In order to rule out this false positive, we utilized gentamicin to shut off gene expression of extracellular *E. coli*.

We tested whether incubation with 100 μg/mL of gentamicin can prevent gene activation by small molecules. *E. coli* harboring the escape device and GFP under P_{BAD} (Figure 2.8A) was incubated with 100 μg/mL of gentamicin for 1 hour or 2 hours before 0.2 % arabinose was added. Then *E. coli* were further incubated for 2 hours. Even when induced, GFP expression of gentamicin-treated *E. coli* was comparable to the uninduced sample (Figure 2.8).

To assess this *in vivo*, the same *E. coli* were incubated with mammalian cells to allow invasion (Figure 2.9A). Then the cells were incubated with the complete growth medium supplemented with 100 μg/mL gentamicin. When inducers were added, GFP expression was comparable to the induced sample without gentamicin treatment after two hours (Figure 2.9) indicating that we were able to control the gene expression of intracellular *E. coli* using extracellularly supplemented inducers.

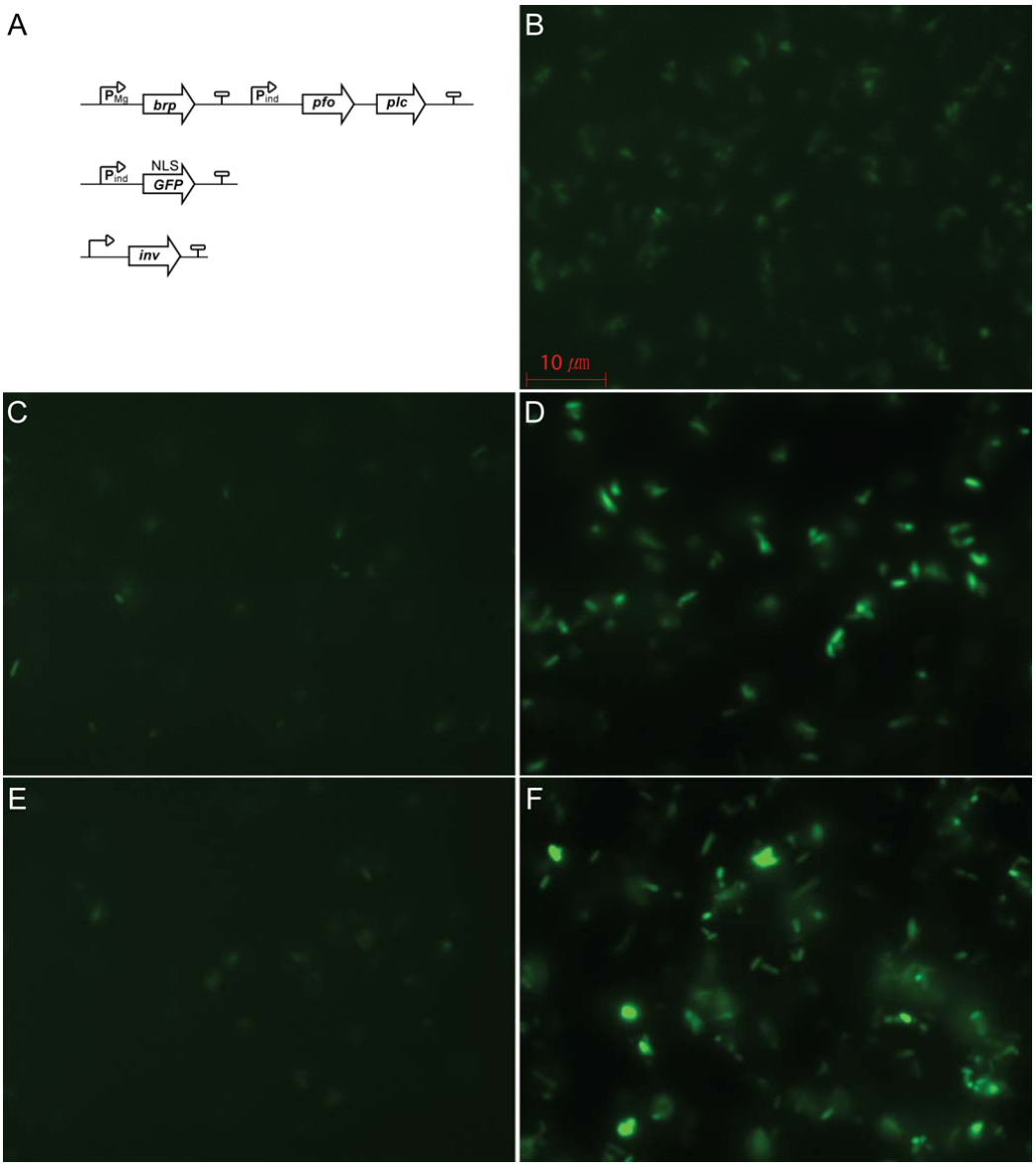

Figure 2.8 Prior incubation of bacteria with gentamicin inhibited the GFP exression when induced

A. Device composition. GFP was placed downstream of P_{BAD}.
B. Uninduced control: no arabinose was added to *E. coli*.
C. Induced with 0.2% arabinose after incubation with 100ug/uL gentamicin for 1 hour. The expression of GFP was inhibited.
D. Induced with 0.2% arabinose without incubation with 100ug/uL gentamicin for 1 hour. The expression of GFP was induced.
E. Induced with 0.2% arabinose after incubation with 100ug/uL gentamicin for 2 hour. The expression of GFP was inhibited.F. Induced with 0.2% arabinose without incubation with 100ug/uL gentamicin for 2 hour. The expression of GFP was induced.

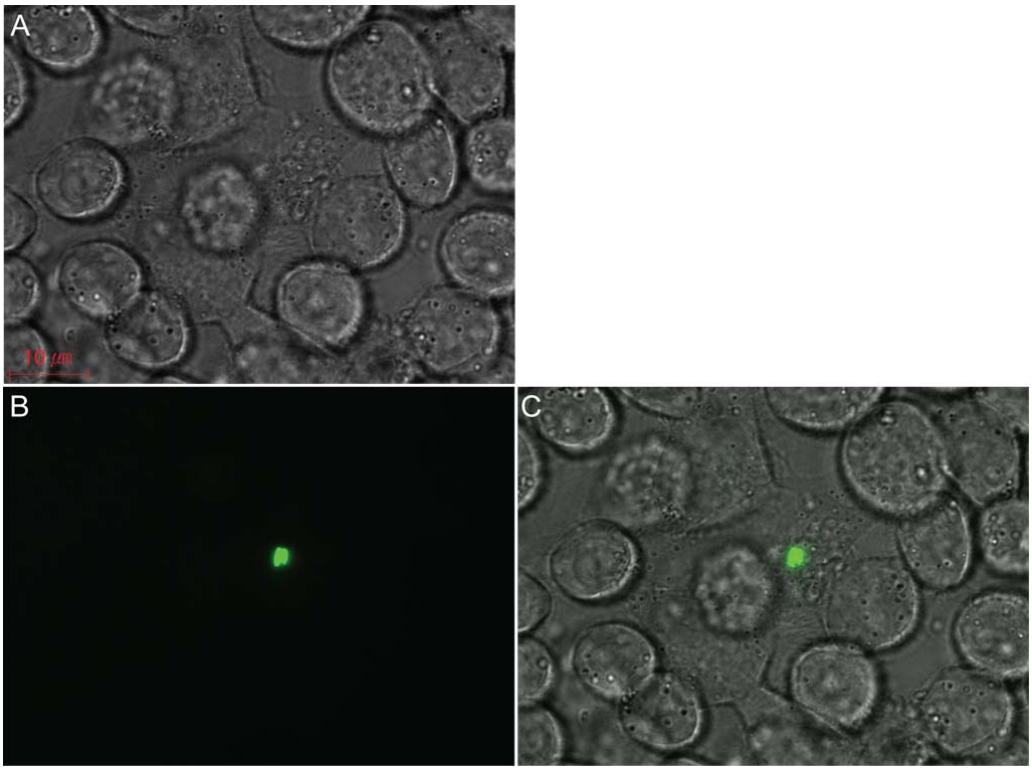

Figure 2.9 GFP expression of *E. coli* inside mammalian cell were induced by 0.2% arabinose supplemented in mammalian cell culture medium

Bacteria with the same device composition as Figure 2.8A were used. The expression of the VL was induced to facilitate the escape from the vacuole prior to invasion. After invasion, mammalian cell culture was treated with gentamicin for 1 hour, and then 0.2% arabinose was supplemented in the medium.

A. Bright field image.

B. The expression of GFP was induced, and the intensity of GFP signal was comparable to induced control in Figure 2.8D and F.

C. GFP and bright field channel were merged.

2.2.2.3 *E. coli* in host cytoplasm released payload in response to small molecules

After obtaining the ability to trigger gene expression from *E. coli* in cytoplasm, we sought to induce expression of inner and outer membrane permeabilization devices and allow cytoplasmic GFP-NLS to be released to cytoplasm of target mammalian cell and localized in nucleus. *E. coli* harboring P_{BAD} driving the inner membrane permeabilization device and *brp*, the VS driving *brp*, and P_{RHM} driving the VLD were incubated with mammalian cells (Figure 2.10A). Bacteria were incubated with mammalian cells to allow invasion. Then they were incubated with 100 μg/mL gentamicin for 1 hour to rule out false positive. When induced, GFP was successfully localized to nucleus (Figure 2.10). Although more controls such as staining nucleus and phagosome would be required, this suggests that our new secretion device is working as expected.

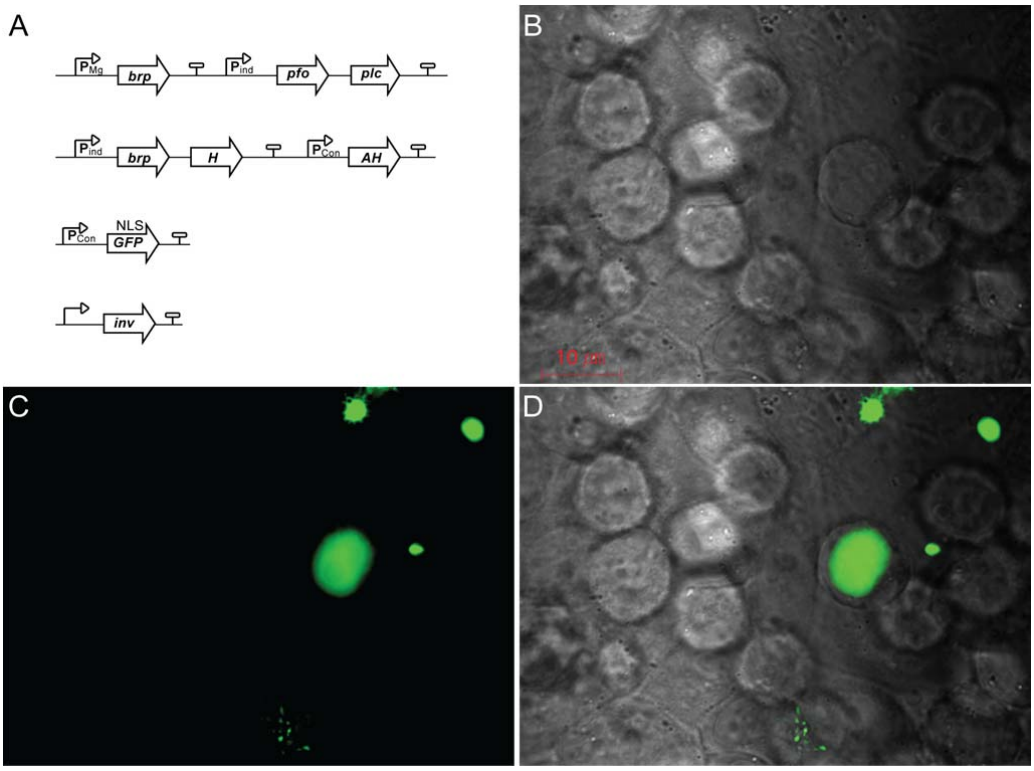

Figure 2.10 GFP-NLS was delivered to nucleus when induced
The vacuole-induced expression of the BRP was designed to facilitate bacteria escape from vacuole by releasing the pre-loaded vacuole lysis device. Addition of 0.2% arabinose was to permeabilize the inner and outer membrane, and release constitutively expressed GFP-NLS, which was localized in the nucleus.
A. Device composition.
B. Bright field image
C. GFP-NLS was released and localized in the nucleus after the addition of arabinose to the medium.
D. Green and bright field channels were merged.

2.3 Discussion

Here we demonstrated that we can engineer *E. coli* to enact a variety of delivery strategies by simply and rationally mixing and matching currently available devices. This provides an additional example that standardization, abstraction, and modularity are powerful and valid engineering principles for biology as well. The removal of *E. coli* by autophagy still remains to be tested.

When we encountered that the TAT signal peptide tagged payloads were not released, we fixed the problem by partially permeabilizing inner and outer membrane of bacteria. Although the device worked as we expected, the delivery process itself was not the ideal way of delivering payloads. Like the payload delivery device, bacterial proteins would have also leaked out of bacteria. Additionally, the stability and viability of membrane permeabilized bacteria would have to be extensively tested. Therefore, another type of secretion system, such as the type III secretion system, must be considered to replace our current design. A type III secretion

system could also obviate BRP by targeting the vacuole lysis device directly to outside. In this case, however, the vacuole sensor device cannot be pre-loaded before they invade the target host cell, and, therefore, the efficiency of escape from vacuole would decrease significantly. Pre-loading of the vacuole lysis device not only increases the efficiency of escape from vacuole, but also makes the payload secretion device compatible with autophagy mediated removal of *E. coli* after the delivery is completed. If the vacuole sensing device or constitutive promoter were driving the expression of the vacuole lysis device, *E. coli* would be able to escape from autophagy multiple times. By pre-loading the vacuole lysis device with a small molecule, *E. coli* can escape from the vacuole only once during the delivery process.

This mode of delivery can be adopted to have more sophisticated behaviors. Genetic circuits or biosensors can be combined or replace the current device, such that *E. coli* can sense the cellular state of target, actuate delivery sequence accordingly, and be removed without human intervention. This mode of delivery maximizes the utility of live *E. coli* as a drug delivery vehicle. Taking advantage of their property of sensing and actuation is what differentiates bacteria based therapeutics from other currently available drug vehicles.

2.4 Material and Methods

2.4.1 Plasmids and Strains

The genetic constructs used in this study were constructed using BglBrick standard assembly [50], a variation on BioBrick standard assembly using the *Bgl*II and *Bam*HI restriction enzymes. To facility part assembly, methylating strains of *E. coli* were employed [51]. All experiments were performed with *E. coli* strains MG1655, MC1061, and derivatives thereof (Table 2.4). Sequences of DNAs used to fabricate composite devices are available in the MIT Registry of Standard Biological Parts [52]. The complete composition of devices is available in Appendix (Table 1.2).

2.4.2 Growth medium and condition

E. coli were grown in Luria Broth (LB) medium for routine molecular biology protocols. Cultures were grown in Luria Broth (LB) for routine cloning. Cultures for experiments were grown in Terrific Broth (TB) supplemented with appropriate antibiotics and 30 mM of $MgSO_4$ (TB + Mg). Cultures were induced with a final concentration of 0.2 % arabinose or 10mM rhamnose in TB. Cultures were grown at 37 °C and 700 rpm (Multitron Standard, INFORS-HT, Bottmingen, Switzerland)

2.4.3 Microscopy of devices

A monolayer of HeLa or U373 MG cells was prepared 24 hours prior to experimentation on an 8-well chambered slide (LabTech) in growth medium (DMEM supplemented with 10% fetal bovine serum (FBS) for HeLa and DMEM supplemented with 1% non-essential amino acids (NEAA), 1 mM sodium pyruvate, and 10% FBS for U373 MG) with penicillin and streptomycin antibiotics. The medium was replaced with fresh medium without antibiotics, and stationary phase bacterial culture (grown in TB + Mg2+) was added to each well. After 80 minutes of incubation at 37 °C, cells were washed twice into growth medium with 100 µg/mL gentamicin, and the slides incubated for a further 3.5 hours before the examination by microscopy. For experiments involving induction with small molecules, the slide was incubated at 37 °C for 1 hour in 100 µg/mL gentamicin supplemented medium after washing twice. Then medium was exchanged with the medium supplemented with 100 µg/µL gentamicin and 0.2% arabinose, and incubated further 2 hours. Images were taken with Zeiss Axiobserver D1 or Zeiss Axiovision Z1 inverted microscope equipped with Hamamatsu 9100-13 EMCCD camera. The delivery efficiency was quantified as the number cells with a green nucleus divided by the number of cells bearing internalized bacteria and/or a green nucleus. To determine cytotoxicity after the 3.5 hour incubation, each well was incubated with PBS containing a final concentration of 4 µM of ethidium homodimer-1 (EthD-1) (Life Technologies) and 2 µM of Hoechst 33342 (VWR) for 10 min at 37 °C. EthD-1 stains the nucleus of membrane permeabilized (dead) cells and Hoechst stains the nucleus of all cells. Cytotoxicity was calculated as the number of EthD-1 stained cells divided by the number of cells bearing internalized bacteria and/or a green nucleus. To stain acidified vacuoles, the medium was exchanged with the growth medium

supplemented with 100 nM of LysoTracker™ Red DND-9 (Molecular Probes) and incubated for 1hr at 37 °C. For imaging GFP induction, the exposure time was set to 5.10 seconds.

2.5 Table

Table 2.1 Plasmids used in experiments

Figure	Label	Plasmid
2.2	VSD(P_{phoP}) driving VLD(degradation tagged *pfo*/*plc*) and BRP, and P_{CON} driving TAT tagged PLD	Bjh2107-BBa_J72118
2.3B	Payload Device	Bjh2313-BBa_J72117
2.3D	VSD(P_{mgrBl}) driving IMP with BRP	Bjh2131-BBa_J72118
	Payload Device	Bjh2313-BBa_J72117
2.4B	PSD with P_{CON} driving VLD(degradation tagged *pfo*/*plc*), and VSD(P_{mgrBl}) driving IMP with BRP	Bjh2402-BBa_J72118
	Payload Device	Bjh2313-BBa_J72117
2.5	PSD with P_{phoP} driving VLD(degradation tagged *pfo*/*plc*), IMP, and BRP	Bjh2087-BBa_J72118
	PSD with P_{CON} driving VLD(degradation tagged *pfo*/*plc*), and VSD(P_{phoP}) driving IMP with BRP	Bjh2347-BBa_J72118
	PSD with P_{CON} driving VLD(degradation tagged *pfo*/*plc*), and VSD(P_{mgrBl}) driving IMP with BRP	Bjh2402-BBa_J72118
	Payload Device	Bjh2313-BBa_J72117
2.6, 2.7	VSD(P_{mgrBl}) driving BRP, and P_{BAD} driving VLD(degradation tagged *pfo*/*plc*)	HK42-BBa_J72118
	VSD(P_{mgrBl}) driving BRP, and P_{RHM} driving VLD(degradation tagged *pfo*/*plc*)	HK45-BBa_J72118
	P_{glpT} driving GFP	jtk2828-BBa_J72147
2.8, 2.9	VSD(P_{mgrBl}) driving BRP, and P_{RHM} driving VLD(degradation tagged *pfo*/*plc*)	HK45-BBa_J72118
	P_{BAD} driven GFP, and P_{CON} driven RFP	HK54-BBa_J72147
2.10	VSD(P_{mgrBl}) driving BRP, and P_{RHM} driving VLD(degradation tagged *pfo*/*plc*)	HK45-BBa_J72118
	P_{BAD} driving IMP with BRP, and P_{CON} driven RFP	HK63-BBa_J72147

Table 2.2 Strains used in experiments

Figure	Strain*
2.2, 2.3B, 2.3D, 2.4B, 2.5	JH-4-C3 (MG1655 Δ*tonB* attP21::P_{flu}-*inv*)
2.6, 2.7, 2.8, 2.9, 2.10	3E9_p1_T6-3 (MG1655 attP21::P_{flu}-*inv,* O16::pcon_repA(ColE2), upp::pcon(23100)_pir)

* Strain modifications were made using standard techniques [55, 56, 57].

Chapter 3

Protein Delivery to Eukaryotic Organisms

3.1 Introduction

Choanoflagellates are the closest known relatives of metazoans [72]. They represent a distinct lineage that evolved separately from metazoans [73]. They are globally distributed and can be found abundantly in both marine and freshwater environments. Over 125 species have been identified, and many of them exist as unicellular or colonial form.

Choanoflagellates are very attractive model organisms for developmental and evolutionary biologists. Interestingly, for some species of choanoflagellates colony formation of unicellular species is induced by factors such as bacteria [74]. They are located in the middle of unicellular and colonial progenitor of metazoans in the evolution tree, and, therefore, may provide answers for evolution from unicellular to multicellular organisms. Despite the scientific opportunities that choanoflagellates can provide, research with these organisms is limited to mostly comparative genomics or phylogenic analysis due to lack of transgenic tools. Therefore, the development of genetic tools for these organisms is very important.

Typically, choanoflagellates have an apical flagellum surrounded by a distinctive collar of actin-filled microvilli. They use this collar to create a current to capture prey such as bacteria. Captured bacteria are then engulfed and reside in the vacuole. The vacuole is fused with a food vacuole where bacteria are digested. Their eating process closely resembles the phagocytosis of bacteria by mammalian cells as described in Chapter 2. Therefore, we attempted to develop a genetic tool by modifying our payload delivery device. In fact, since the delivery process is similar to many other organisms that feed on bacteria, we anticipate that a transgenic tool developed here can be easily adopted for other organisms that share similar feeding process.

3.2 Result

3.2.1 Analysis of device compatibility with choanoflagellates

We analyzed each device whether they were compatible with choanoflagellates. As for the payload device, SV 40 NLS tagged fluorescent protein has been shown to localize in nucleus in various species including yeast, Xenopus, Drosophila, plants, and mammals [75, 76, 77, 25]. Therefore, it was reasonable to keep our current payload device for the initial experiment. The invasion device can be ignored as long as choanoflagellates can actively feed on our chassis, *E. coli* MG1655. The performance of the self-lysis device and BRP would be unaffected because their target substrates remain the same, the inner membrane, peptidoglycan layer, and outer membrane, respectively. The performance of the vacuole lysis device, however, can be affected because it is unknown whether PFO or PLC would have the similar activity on the vacuole membrane of choanoflagellates. The performance of the vacuole sensor device is also unknown since magnesium concentration in the vacuole of choanoflagellates is unknown. We continued with our best payload delivery device for initial experiment, and we will troubleshoot after identifying possible failures.

3.2.2 Viability of choanoflagellates at various temperatures

For better delivery efficiency, it was logical that the optimal temperature for *E. coli* is desired, since the components of the payload delivery device performs naturally at 37 °C. Typically many species of choanoflagellates are cultured at 25 °C. Thus, it was important to assess whether the viability of choanoflagellates is affected when cultured in elevated temperature. We measured viability of *Salpingoeca rosetta*after incubating them at 25 °C, 37 °C, and 50 °C for 24 hours (Figure 3.1). Even when they were cultured at 37 °C for 24 hours, their viability was not altered. Therefore, we decided to co-incubate bacteria and choanoflagellates at 37 °C during the payload delivery experiment.

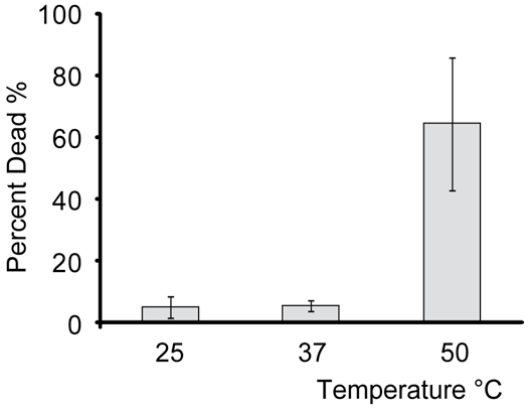

Figure 3.1 Viability of *Salpingoeca rosetta* cultured at different temperature for 24 hours

The viability of *S. rosetta* at 37 °C was minimal.

3.2.3 Initial test suggested that faster response to internalization is required

To address whether the invasion device can be replaced by natural uptake by choanoflagelles, we mixed *Monosiga brevicollis* with *E. coli* bearing the payload device and lacking the invasion device, and incubated them at 37 °C. Indeed, the uptake of *E. coli* was confirmed (data not shown).

To examine whether the vacuole sensor device can properly function in the vacuole of *Monosiga brevicollis*, *E. coli* bearing the payload device and mammalian optimized version of the payload delivery device were fed to *Monosiga brevicollis*. However, the payload was concentrated in the food vacuole within an hour (Figure 3.2). Compared to payload delivery in mammalian cells, the speed of vacuole trafficking to the food vacuole is much faster than the time required for the VS to activate other devices. Therefore we sought to modify the vacuole sensing device.

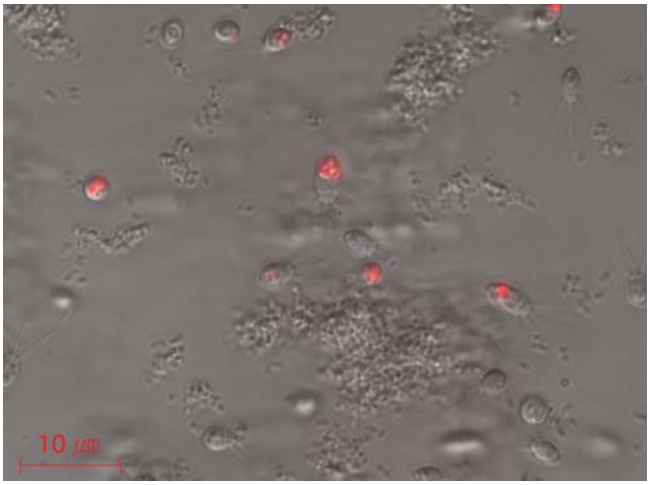

Figure 3.2 *E. coli* were engulfed by *Monosiga brevicollis* and concentrated in food vacuole

E. coli expressing RFP were engulfed by choanoflagellates and concentrated in food vacuole, where they were digested.

3.2.4 Working VSD was identified

Developing the VSD for mammalian cells suggested that it would be difficult and time-consuming to build and test a new vacuole sensing device that can sense the vacuole of choanoflagellates with unknown characteristics and activate the self-lysis device within a few minutes before the phagosomal vacuole fuses with the food vacuole. Unlike the payload delivery to mammalian cells, our goal is not to build a delivery system that can specifically sense the vacuole environment or can deliver with high efficiency with lowest MOI possible. Specific sensing of the vacuole environment is not required to achieve our goal. In addition, MOI of bacteria to choanoflagellates are not a significant issue, since they naturally interact with bacteria in habitat. For our application, it would not matter if bacteria lyse outside of choanoflagellates. Our hypothesis was that feeding pre-induced payload delivery device would give higher delivery efficiency. We picked a version of the payload delivery device that was predicted to be pre-lysing from Chapter 1 (Figure 3.3A). Indeed, their spherical shape indicated that their structural integrity has been compromised (Figure 3.4B, C, D). When these *E. coli* were fed to *Monosiga brevicollis*, GFP and RFP was distributed in the cytoplasm, indicating that this version of payload delivery device was able to self-lyse in time and degraded the vacuole membrane (Figure 3.4). However, GFP-NLS did not localize in nucleus. Choanoflagellates with RFP in cytoplasm and GFP-NLS concentrated in the nucleus were not observed,suggesting that SV 40 NLS is not functional in *Monosiga brevicollis*. Since the localization of protein failed, we used the deconvolution fluorescent microscopy to confirm that GFP and RFP are filled in the cytoplasmic space [78].

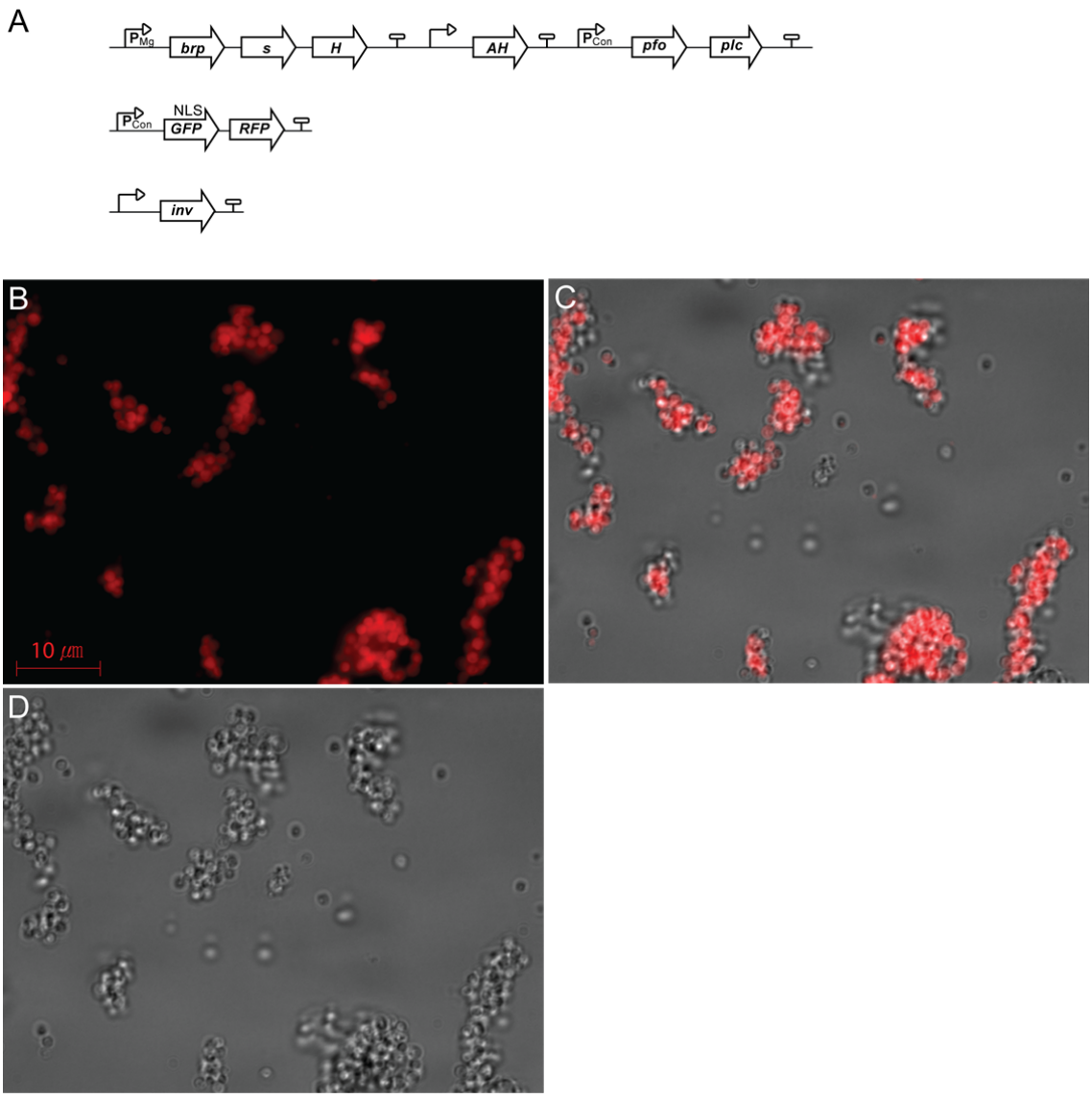

Figure 3.3 Spherical shape of *E. coli* carrying the payload delivery device

A. The composition of device was identical to the device used for the mammalian cells, except for the vacuole sensing device. The device with higher basal level expression was used to ensure their fast self-lysis within the vacuole.

B. Images of RFP expressing bacteria with the payload delivery device were taken prior to feeding choanoflagellates. The spherical shape of bacteria indicated that their structure integrity was compromised due to higher basal expression level of the vacuole sensing device used here.

C. RFP and bright field images were merged.

D. Bright field image

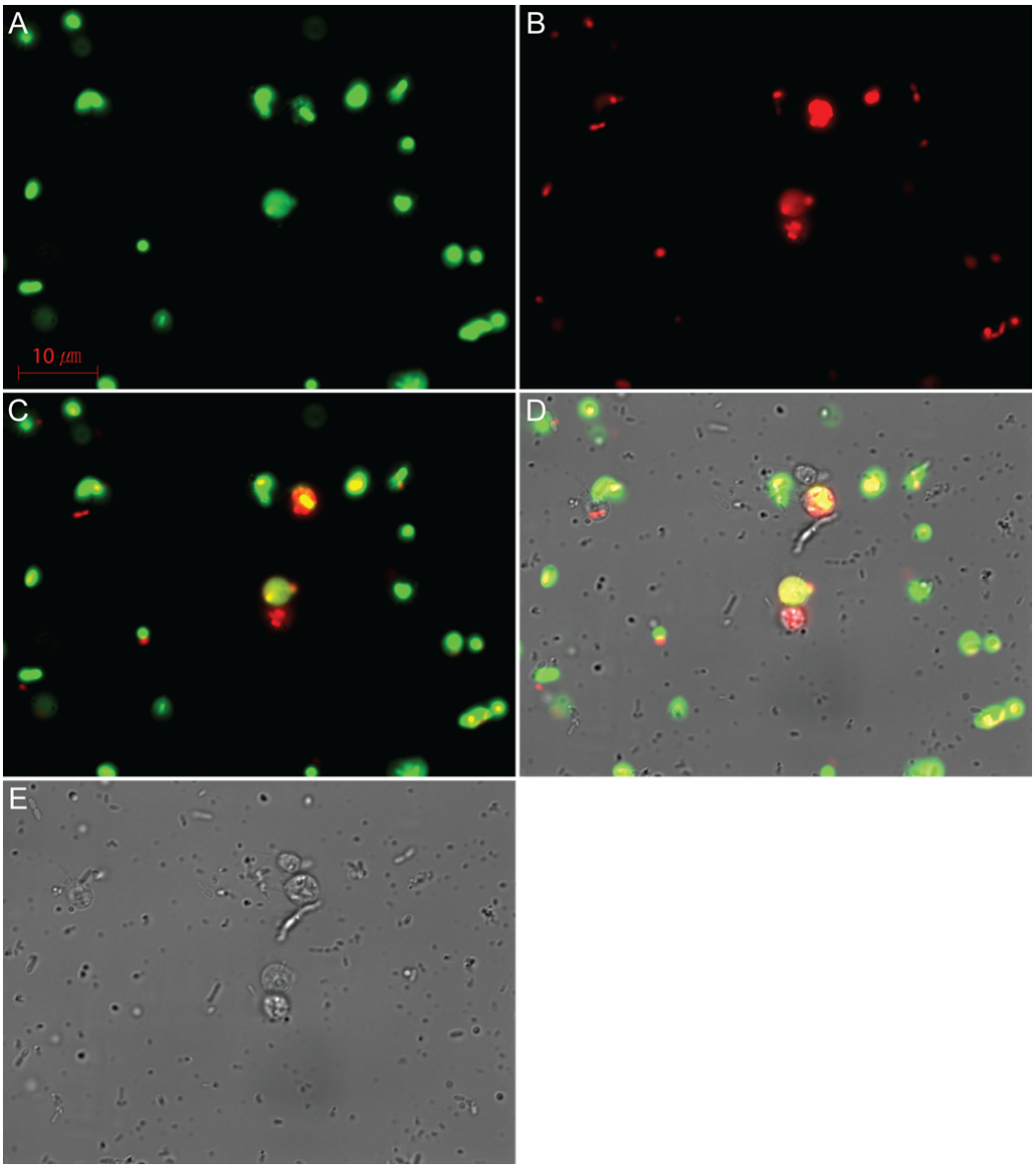

Figure 3.4 GFP-NLS and RFP may have been delivered to cytoplasm of choanoflagellates

Both GFP-NLS and RFP were distributed in the cytoplasm of a choanoflagellate in the center of the image. Without localization of GFP-NLS, the success of the payload delivery cannot be confirmed.
A. For the choanoflagellate in the center, GFP-NLS was distributed in the cytoplasm.
B. RFP was distributed in the cytoplasm.
C. GFP-NLS and RFP images were merged.
D. GFP-NLS, RFP, and bright field images were merged.
E. Bright field image

3.2.5 VLD only worked in M. ovata and brevicollis

PFO is the primary functional component of the vacuole lysis device, and has selective activity on membranes which contain cholesterols [79]. This raised the question of whether the vacuole lysis device would be active on the membrane of choanoflagellates. According to Jon Grabenstatter from Harvard University, there is no cholesterol in *Monosiga*. There is a trace amount of cholesterol (C27 delta 5) and a substantial concentration of C27 delta 5, 22 sterol in *Salpingoeca*. The main sterol in both choanoflagellates is C27 delta 5, 7, 22 (personal communication, January 30, 2012). Since little was known for other species, we set out to test delivery on six different species of choanoflagellates. Among those, we only observed RFP delivery to cytoplasm for *Monosiga brevicollis* and *Monosiga ovata*.

3.2.6 Payload delivery worked on Naegleria, but localization failed

In parallel to choanoflagellates, the payload delivery device was tested on another genetically intractable organism of our interest, the protozoan *Naegleria gruberi*. They feed on bacteria, and can transform their cellular state from amoeba state to either flagellated state or encysted state within minutes [80]. When we tried the payload delivery, RFP was delivered to cytoplasm (Figure 3.5). According to Lillian Fritz-Laylin from University of California, San Francisco, this image was similar to syringe-loaded *Naegleria* with proteins (personal communication, February 22, 2012). However, the localization of GFP-NLS failed.

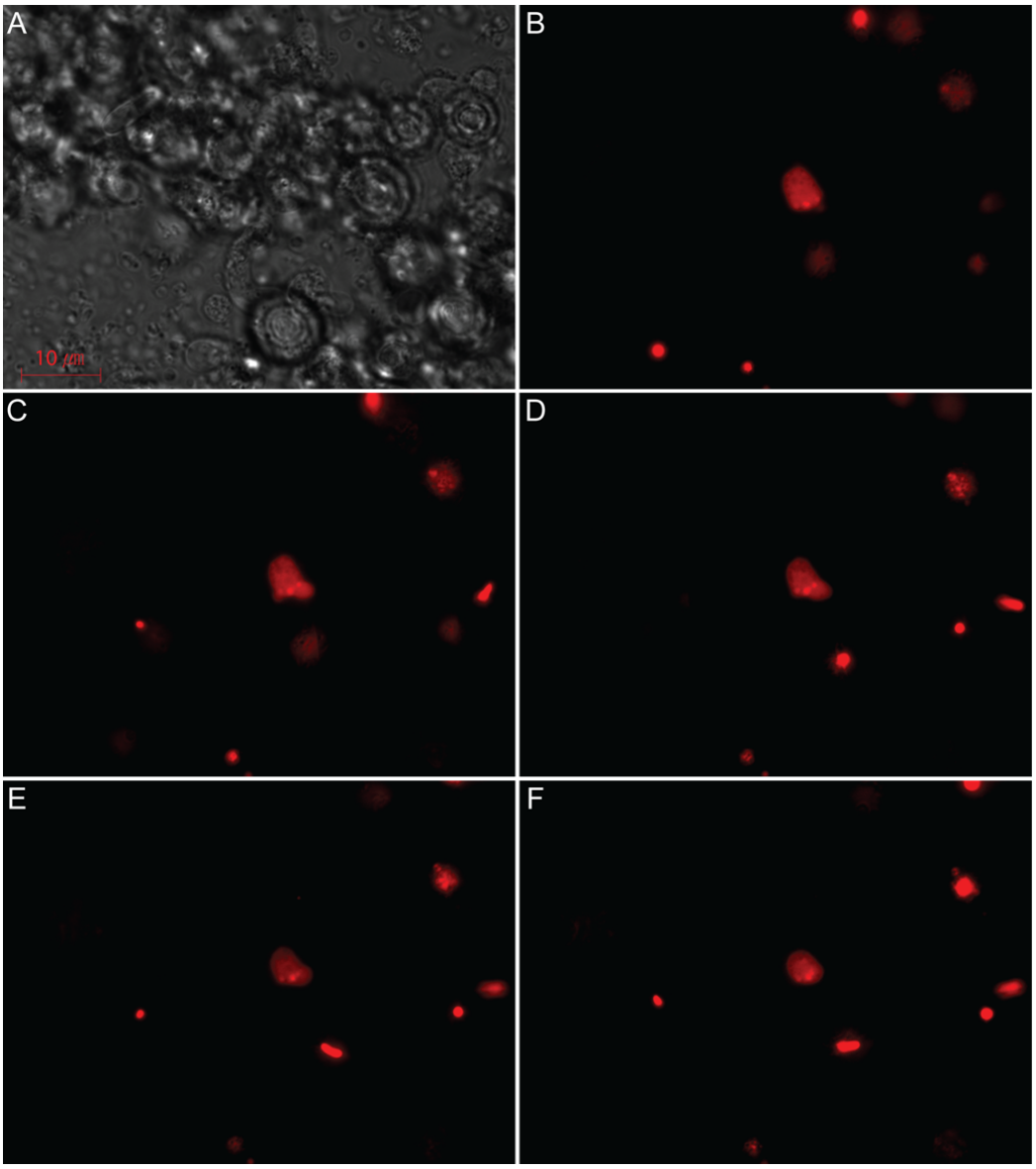

Figure 3.5 RFP may have been delivered to cytoplasm of *Naegleria gruberi*
RFP was distributed in the cytoplasm of *Naegleria gruberi* in the center of the image. The amoeba's shape is distorted as it crawled across the surface of the dish. Images were taken in 10 second interval.
A. Bright field
B. T=0 sec.
C. T=10 sec.
D. T=20 sec.
E. T=30 sec.
F. T=40 sec.

3.2.7 Payload delivery to Dictyostelium discoideum

Localization of payload would provide concrete evidence that delivery was successful. Since we cannot draw the line whether delivery worked or not, we attempted to deliver to another organism that can provide more useful information, *Dictyostelium discoideum*. Because this organism is genetically tractable, we now have means to better assess the performance of our devices. As an initial experiment, we tried the payload deliver device on *Dictyostelium discoideum* and were able to deliver RFP to its cytoplasm (Figure 3.6).

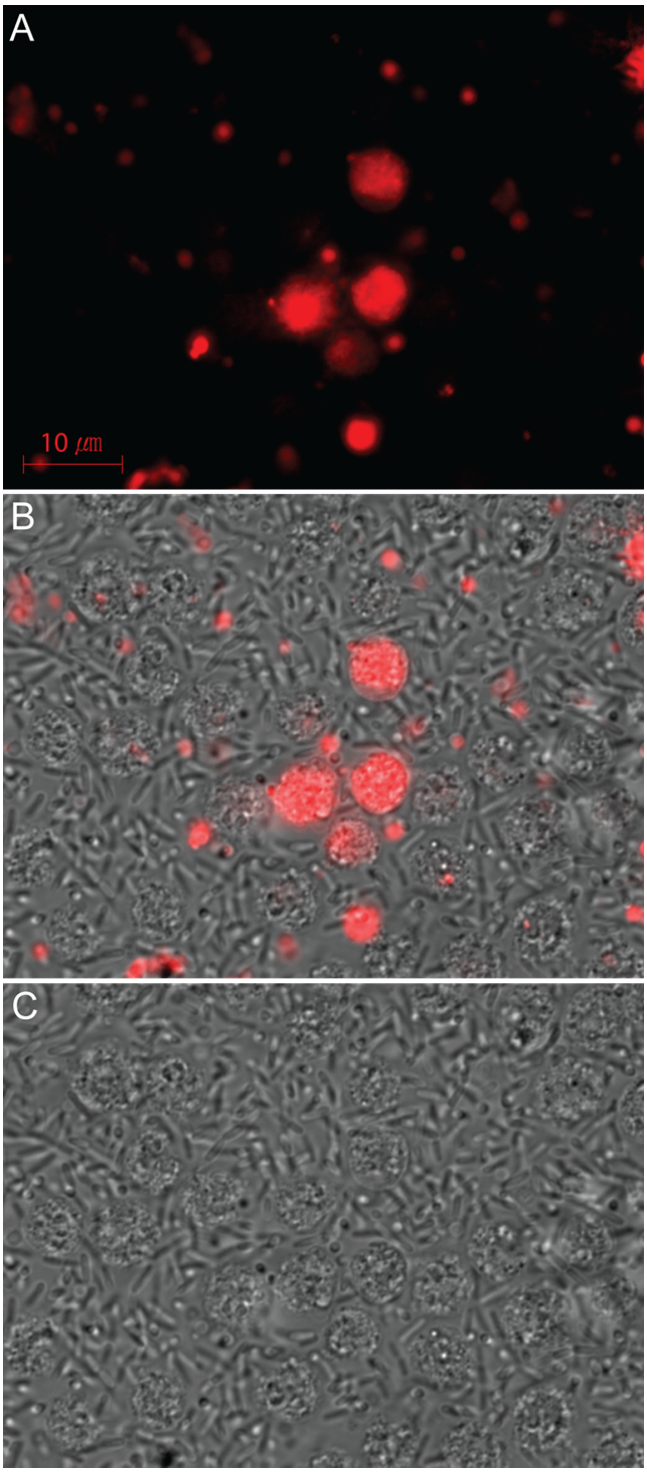

Figure 3.6 RFP may have been delivered to cytoplasm of *Dictyostelium discoideum*

A. RFP was distributed in the cytoplasm of *Dictyostelium* (spherical shape).
B. RFP and bright field images were merged.
C. Bright field image

3.3 Discussion

Payload delivery to Choanoflagellates remains inconclusive. It was difficult to troubleshoot the system since little is known about their biology. As an alternative, we tested the payload delivery device on the organism that is already genetically tractable, *Dictyostelium discoideum*. EIF6 and numA fused GFP were previously demonstrated to be localized to nucleus [81, 82]. By delivering these proteins using our device, we may be able to show localization to nucleus and unambiguously confirm the successful delivery. The next step would be to clone these genes and try delivering these.

3.3.1 Consideration when building payloads

Another consideration when designing the payload delivery experiments is the toxicity of payload to *E. coli* or interference with lysis. H2B [83] and Lifeact [84] are good examples. A constitutive expression of H2B-GFP fusion protein caused slow growth of *E. coli*, and self-lysis was diminished when lifeact-GFP was constitutively expressed. For some cases, fluorescence of GFP was decreased when proteins were fused. Therefore, stability, toxicity, and activity of payload must be considered when designing or identifying possible candidates for payloads.

3.3.2 Identifying NLS of choanoflagellates

There are several biochemical experiments, such as identifying nuclear localization signals, needed to address the challenges encountered. To identify nuclear localization signals in choanoflagellates, a GFP fusion library of fragmented nuclear proteins of choanoflagellates can be generated and then screened.

3.3.3 VLD and membrane composition of choanoflagellates

Perfringolysin O is known to selectively act on membranes which contain cholesterols. The payload delivery device, however, seems have worked on *Monosiga* species, although a concrete evidence was still required. This was surprising since *Monosiga* have been shown to have no cholesterol in membrane. We expected at first that the payload delivery would work better on *Salpingoeca* species since they had cholesterol within their membrane. It could be that some unknown types of sterol, which exist in *Monosiga* but not in *Salpingoeca*, could be sufficient for perfringolysin O activity. More sophisticated mass spectroscopy analysis and other biochemical experiments are needed to answer this question.

3.3.4 Difficulties in microscopy

To confirm nuclear localization, it is necessary to identify the nucleus. DNA intercalating dyes, such as DAPI or Hoechst, can be used for such purposes [85, 86]. For the organisms tested, however, it is not that simple. For instance, these dyes stain not only the nucleus but also bacteria-containing vacuoles and food vacuoles by intercalating into bacterial DNA in those vacuoles. In order to solve this, we can

co-stain the cells with LysoTracker™ (Molecular Probes), which stains the vacuole and food vacuole. The nucleus would be only stained with DAPI, where other vacuoles are stained with DAPI and LysoTracker™. Another strategy would be to utilize immunofluorescence against nuclear protein, although it would be cumbersome and laborious

3.4 Material and Methods

3.4.1 Plasmids and Strains

Genetic devices used in this study were constructed using BglBrick standard assembly [50]. *Bgl*II- and *Bam*HI-methylating strains of *E. coli* were used for cloning [51]. MG1655 and derivatives were used for payload delivery experiments. *Monosiga ovata*, *Monosiga brevicollis*, *Monosiga gracilis*, *Salpingoeca rosetta*, *Salpingoeca infusionum, Salpingoeca napiformis,* and *Salpingoeca pyxidium* were provided by Nicole King laboratory at University of California, Berkeley. *Dictyostelium discoideum* AX2 was a gift from Daniel Fletcher laboratory at University of California, Berkeley. *Naegleria gruberi* NEG and *Klebsiella aerogenes* were provided by Lillian Fritz-Laylin from University of California, San Francisco.

3.4.2 Growth medium and condition

The complete protocols for handling choanoflagellates are described at ChoanoWiki [87]. The protocol for *Naegleria gruberi* is adopted from the previous study [80]. The protocols are briefly summarized below.

3.4.2.1 Culturing of *E. coli*

Cultures were grown in Luria Broth (LB) for routine cloning. Cultures for payload delivery experiments were grown in Terrific Broth supplemented with appropriate antibiotics and 30 mM of $MgSO_4$ (TB + Mg). All *E. coli* cultures were grown at 37 °C and 700 rpm (Multitron Standard, INFORS-HT, Bottmingen, Switzerland)

3.4.2.2 Preparation of the feedstock of *Klebsiella aerogenes*

A colony of *Klebsiella aerogenes* was inoculated into 50 mL of Antibiotic Medium 3 (Difco), and grown overnight at 30 °C with shaking. The overnight culture was pelleted at 5,000 rpm for 10 min. The pellet was washed once with 50 mL of Tris-Mg buffer. Then it was resuspended in 5 mL of Tris-Mg buffer, and stored at 4 °C.

3.4.2.3 Cereal grass medium

Per a liter of boiled natural seawater5 g of Ward's cereal grass (Scholar Chemistry #9448606) was added. It was cooled down, and the macroscopic cereal grass particles were removed by vacuum filtering twice through Buchner (ceramic) funnel with a double layer of # 1 Whatman (cat# 1001 150). This filtered medium was sterile filtered through a .22 µm filter. For various percentages of cereal grass medium, appropriate amount of cereal grass medium was diluted in sterilized natural sea water.

3.4.2.4 Sea water

Natural seawater was sterile filtered through a .22 µm filter.

3.4.2.5 Fresh cereal grass medium

For fresh water living choanoflagellates, such as *Monosiga ovata* or *Salpingoeca napiformis*, natural seawater was replaced by distilled water, and the rest of protocol followed the same protocol as the cereal grass medium. For various percentages of fresh cereal grass medium, appropriate amount of fresh cereal grass medium was diluted in sterilized distilled water.

3.4.2.6 Organic enrichment medium

Thepeptone-yeast solution (0.4 % protease peptone; 0.08 % yeast extract, in distilled water) was diluted 200-fold in sterile sea water, and then sterile filtered through a .22 µm filter.

3.4.2.7 Growth medium for *Dictyostelium discoideum*

The growth medium was prepared by dissolving 26.55 g of HL5-C Medium with Glucose (catalog number HLC0102, Formedium LTD, Hunstanton, England) per 1 L of distilled water, and then it was sterilized by autoclave.

3.4.2.8 Tris-Mg buffer for *Naegleria gruberi*

The final concentration of 2 mM tris was prepared by dilution of a stock 0.1 M tris, pH 7.6, and then supplemented with 10 mM of $MgSO_4$. The buffer was sterile filtered through a .22 µm filter.

3.4.2.9 Preparation of NM agar plates

Per liter of distilled water, 2 g of Difco Bacto-peptone, 2 g of dextrose, 1.5 g of K_2HPO_4, 1 g of KH_2PO_4, and 20 g of Difco Bacto-agar were dissolved., It was then autoclaved, and poured into petri dish.

.

3.4.2.10 Culturing of choanoflagellates

All cultures were grown in 100 mm tissue culture plates for adherent choanoflagellates or 25 cm^2 tissue culture flasks for suspension choanoflagellates without shaking. For adherent choanoflagellates, the plate bottom was scrapped prior to passaging. All of choanoflagellates were cultured at room temperature, except for *Salpingoeca pyxidium* which was cultured at 15 °C.

3.4.2.10.1 Monosiga ovata

Cultures were grown in 25 % of fresh cereal grass medium. Cultures were split 1:10 approximately every four days with a total volume of 20 ml

To prepare for the payload delivery experiments, cultures were grown in 50 mL scale, and filtered through 3 μm filter. Bacteria were passed through and choanoflagellates remained in the filter. Then they were washed by passing 25 % fresh cereal glass medium through the filter. Choanoflagellates were collected by resuspending them with 5 mL of 25 % fresh cereal glass medium. The choanoflagellate suspension was transferred to each well of 8-well chambered slides (LabTech) in 500 µL aliquots.

3.4.2.10.2 Monosiga brevicollis

Cultures were grown in 100 % cereal grass medium. This particular culture was a monoxenic line with feeder bacteria *Enterobacter aerogenes*. Cultures were split 1:5 every two days with a total volume of 15 mL.

To prepare for the payload delivery experiments, cultures were grown in 50 ml scale, scrapped, and filtered through 40 μm cell strainer, which captures clumps of bacteria, then the filtrate was filtered through 8 um filter. The bacteria have a tendency to clump. Therefore, bacteria remained in the filter, while choanoflagellates passed through the filter. The filtrate was collected. The choanoflagellate suspension was transferred to each well of 8-well chambered slides in 500 µL aliquots.

3.4.2.10.3 Monosiga gracilis

Cultures were grown in 10 % cereal grass medium. Cultures were split 1:25 approximately every seven days with a total volume of 25 mL.

To prepare for the payload delivery experiments, cultures were grown in 50 mL scale, scrapped, and filtered through 3 um filter. Bacteria passed through the filter, while choanoflagellates remained in the filter. Then they were washed by passing sea water through the filter. Choanoflagellates were collected by resuspending them with 5 mL of 10 % cereal glass medium. The choanoflagellate suspension was transferred to each well of 8-well chambered slides in 500 µL aliquots.

3.4.2.10.4 Salpingoeca rosetta

Cultures were grown in 100 % cereal grass medium. This particular culture was a monoxenic line with feeder bacteria *Algoriphagus machipongonensis*. Cultures were split 1:5 every two days with a total volume of 20 mL.

To prepare for the payload delivery experiments, cultures were grown in 50 mL scale. Cultures were then concentrated by centrifugation at 4000 g for 15 minutes at 4 °C. Choanoflagellates were separated from bacteria by density gradient centrifugation using Percoll as following. Choanoflagellates were layered over 2 mL of 10 % Percoll column in sorbitol sea water. The column was centrifuged for 10 minutes at 1000 g at room temperature. Chaonoflagellates were collected as a pellet after removing supernatant. The pellet was resuspended in cereal grass medium. The choanoflagellate suspension was transferred to each well of 8-well chambered slides in 500 µL aliquots.

3.4.2.10.5 Salpingoeca infusionum

Cultures were grown in 10 % cereal grass medium. Cultures were split 1:10 every two days with a total volume of 20 mL.

To prepare for the payload delivery experiments, cultures were grown in 50 mL scale, scrapped, and filtered through 3 μm filter. Bacteria passed through the filter, while choanoflagellates remained in the filter. Then they were washed by passing sea water through the filter. Choanoflagellates were collected by resuspending them with 5 ml of 10 % cereal glass medium. The choanoflagellate suspension was transferred to each well of 8-well chambered slides in 500 μL aliquots.

3.4.2.10.6 Salpingoeca napiformis

Cultures were grown in 25 % fresh cereal grass medium. Cultures were split 1:20 every two days with a total volume of 20 mL.

To prepare for the payload delivery experiments, cultures were grown in 50 mL scale, and filtered through 8 μm filter. Bacteria passed through the filter, while choanoflagellates remained in the filter. Then they were washed by passing distilled water through the filter. Choanoflagellates were collected by resuspending them with 5 mL of 25% fresh cereal glass medium. The choanoflagellate suspension was transferred to each well of 8-well chambered slides in 500 μL aliquots.

3.4.2.10.7 Salpingoeca pyxidium

Cultures were grown in organic enrichment medium at 15 °C. Cultures were split 1:25 every two weeks with a total volume of 25 mL.

To prepare for the payload delivery experiments, cultures were grown in 50 mL scale, and centrifuged at 4000 g for 15 min at 4 °C. The supernatant was removed, and pellets were resuspended in organic enrichment medium. The choanoflagellate suspension was transferred to each well of 8-well chambered slides in 500 μL aliquots.

3.4.2.11 Culturing of *Dictyostelium discoideum*

Dictyostelium discoideum AX2 was obtained on a 100 mm petri plate. The plate was scrapped after adding 5 mL of the growth medium onto the plate. From the scrapped suspension, 500μL was mixed into 50 mL of the growth medium supplemented with penicillin and streptomycin antibiotics, and plated on a 150 mm tissue culture grade petri dish. They were incubated at room temperature. Then, $5x10^4$ amoeba was split into a new plate when they reach ~10^7.

To prepare for payload delivery experiments, the growth medium in liquid culture plate was discarded, and the plate was washed twice with 10 mL of fresh growth medium without antibiotics. Then, the culture plate was scrapped after adding 5 mL of fresh growth medium without antibiotics. The choanoflagellate suspension was transferred to each well of 8-well chambered slides in 500 μL aliquots.

3.4.2.12 Culturing of *Naegleria gruberi*

To culture them on edge plates, 200 µL of saturated culture of *Klebsiella aerogenes* were plated on NM agar plate 24 hours prior to inoculation of *Naegleria gruberi* to prepare a lawn of bacteria. Naegleria gruberi was inoculated on one end of the plate, parafilmed, and incubated at room temperature. The amoebae propagated across the plate as they feed on *Klebsiella. aerogenes*. Amoebae in the advancing edge became encysted as they depleted the lawn of bacteria. *Naegleria gruberi* on edge plate can be stored for months if the agar is not dried out.

To culture them in liquid culture, one tenth of *Naegleria gruberi* (either cyst or amoeba) on 100 mm petri dish was scrapped off the NM agar edge plate, resuspended in 50 mL of the Tris-Mg buffer, and plated on a 100 mm tissue culture grade petri dish. They were incubated at room temperature, and 100 µL of the feedstock of *Klebsiella aerogenes* was added to the liquid culture as needed or every two days. Then, $5x10^4$ amoeba was split into a new plate when they reach ~10^7 per plate.

To prepare for payload delivery experiments, the Tris-Mg buffer in liquid culture plate was discarded. The plate was washed twice with 10 mL of Tris-Mg, and resuspended with 5 mL of Tris-Mg. The plate was scrapped and 500 µL aliquot of amoeba suspension was transferred to each well of 8-well chambered slide.

3.4.3 Microscopy of devices

Each well of 8-well chambered slides was supplemented with 30 mM $MgSO_4$, and 0.5 µL of saturated culture of bacteria was added to each well of 8-well chambered slides. The slides were examined by microscopy after four hours of incubation at 37 °C. For adherent choanoflagellates or amoeba, medium in each well is replaced by new medium with gentle and slow pipetting. Images were taken with Zeiss Axiobserver D1 or Zeiss Axiovision Z1 inverted microscope equipped with Hamamatsu 9100-13 EMCCD camera.

3.4.4 Measuring viability of choanoflagellates

Propidium iodide (PI) was used to stain dead choanoflagellates which had red fluorescent signal [88]. A culture of choanoflagellates was incubated with 10 µg/ml of PI for 15 min at room temperature in the dark. Choanoflagellates were transferred to hemocytometer after adding 4% formaldehyde. The choanoflagellates with red fluorescent signal were counted under the UV light by microscopy. The total number of choanoflagellates was counted in bright field. Viability of choanoflagellates was calculated by dividing red choanoflagellates by the total number of choanoflagellates.

3.5 Table

Table 3.1 Plasmids used in experiments

Figure	Label	Plasmid
3.2	PDD with P_{CON} driving VLD(degradation tagged *pfo*/*plc*) and VSD(P_{mgrBl}) driving a SLD(λ) with BRP	Bjh2399-BBa_J72118
	Payload Device	Bjh2313-BBa_J72117
3.4, 3.5, 3.7	PDD with P_{CON} driving VLD(degradation tagged *pfo*/*plc*) and VSD(P_{mgtCBl}) driving a SLD(λ) with BRP	Bjh2400-BBa_J72118
	Payload Device	Bjh2313-BBa_J72146
3.6	PDD with P_{CON} driving VLD(degradation tagged *pfo*/*plc*) and VSD(P_{mgtCBl}) driving a SLD(λ) with BRP	Bjh2400-BBa_J72118
	P_{CON} driven RFP	Bca1144-BBa_J72148

Table 3.2 Strains used in experiments

Figure	Strain*
3.2, 3.6	MG1655
3.4, 3.7	JTK186E (MG1655 upp::pcon(23100)_pir)
3.5	3E9_p1_T6-3 (MG1655 attP21::P_{flu}-*inv,* O16::pcon_repA(ColE2), upp::pcon(23100)_pir)

* Strain modifications were made using standard techniques [55, 56, 57].

Chapter 4

Concluding Remarks

The payload delivery device project was initiated as a part of the tumor-destroying bacterium testbed [89, 90]. The proof of concept of tumor-specific invasion of *E. coli* was demonstrated by my dissertation advisor [31, 91]. I was responsible for developing a device that can make *E. coli* to efficiently deliver payloads to the cytoplasm of target cells after invasion. While doing so, we were to develop a design strategy for robust engineering of biology.

I demonstrated that the well-established engineering principles such as standardization, modularity, and abstraction can be applied to engineering of complex biological systems. The time, costs, and efforts in both design and experiments were reduced. It was possible to efficiently troubleshoot unforeseen device malfunctioning based on diagnosis. While successful qualitatively, however, the process uncovered key limitations to our design theory, particularly around our ability to encapsulate and predict quantitative function, and the affects of load and stress on the cell.

We further engineered *E. coli* to have different delivery behavior that could be useful for many applications. The devices built for the payload delivery device were rearranged, and different delivery behaviors were achieved. Because each device is connected and operated by transcriptional control, existing promoters or newly available genetic circuits can be placed together with our devices for more interesting and complex delivery behaviors.

I then expanded the application where the payload delivery device to non-therapeutic applications. We sought to modify the payload delivery device into a transgenic tool for genetically intractable organisms that feed on bacteria. However, this proved more difficult than expected. The limited knowledge about the biology of choanoflagellates made it very difficult to troubleshoot, because we could not provide a good solution to confronted problems.

In conclusion, we explored the design strategy for synthetic biology. Our understanding of the full scope of function exerted by introduced genetic elements remains limited. Although ongoing efforts [92] seek to address gaps in our knowledge, we cannot currently prescribe specific expression levels with confidence or predict how effects on cellular load and stress may impact cellular growth or genetic stability. However, by refocusing our efforts on elucidating formal methods of describing and predicting such phenomena, we ultimately can increase the robustness of our designs and our ability to reliably meet design specifications in genetic engineering projects.

References

1. Khalil, A., & Collins, J. (2010). Synthetic biology: applications come of age. *Nat. Rev. Genet.*, **11**(5), 367-79.

2. Endy, D. (2005). Foundations for engineering biology. *Nature*, **438**(7067), 449-53.

3. Purnick, P., & Weiss, R. (2009). The second wave of synthetic biology: from modules to systems. *Nat. Rev. Mol. Cell Biol.*, **10**(6), 410-22.

4. Prather, K., & Martin, C. (2008). De novo biosynthetic pathways: rational design of microbial chemical factories. *Curr. Opin. Biotechnol.*, **19**(5), 468-74.

5. Tabor, J., Salis, H., Simpson, Z., Chevalier, A., Levskaya, A., Marcotte, E., Voigt, C., & Ellington, A. (2009). A synthetic genetic edge detection program. *Cell*, **137**(7), 1272-81.

6. Wang, B., Kitney, R., Joly, N., & Buck, M. (2011). Engineering modular and orthogonal genetic logic gates for robust digital-like synthetic biology. *Nat Commun*, **2**, 508.

7. Xie, Z., Wroblewska, L., Prochazka, L., Weiss, R., & Benenson, Y. (2011). Multi-input RNAi-based logic circuit for identification of specific cancer cells. *Science*, **333**(6047), 1307-11.

8. Aubel, D., & Fussenegger, M. (2010). Mammalian synthetic biology--from tools to therapies. *Bioessays*, **32**(4), 332-45.

9. Ellis, T., Adie, T., & Baldwin, G. (2011). DNA assembly for synthetic biology: from parts to pathways and beyond. *Integr Biol (Camb)*, **3**(2), 109-18.

10. Andrianantoandro, E., Basu, S., Karig, D., & Weiss, R. (2006). Synthetic biology: new engineering rules for an emerging discipline. *Mol. Syst. Biol.*, **2**, 2006.0028.

11. Keasling, J. (2008). Synthetic biology for synthetic chemistry. *ACS Chem. Biol.*, **3**(1), 64-76.

12. Lou, C., Liu, X., Ni, M., Huang, Y., Huang, Q., Huang, L., Jiang, L., Lu, D., Wang, M., Liu, C., Chen, D., Chen, C., Chen, X., Yang, L., Ma, H., Chen, J., & Ouyang, Q. (2010). Synthesizing a novel genetic sequential logic circuit: a push-on push-off switch. *Mol. Syst. Biol.*, **6**, 350.

13. Courvalin, P., Goussard, S., & Grillot-Courvalin, C. (1996). Gene transfer from bacteria to mammalian cells. *C. R. Acad. Sci. III, Sci. Vie*, **318**(12), 1207-12.

14. Yuhua, L., Kunyuan, G., Hui, C., Yongmei, X., Chaoyang, S., Xun, T., & Daming, R. (2001). Oral cytokine gene therapy against murine tumor using attenuated *Salmonella typhimurium*. *Int. J. Cancer*, **94**(3), 438-43.

15. Larsen, M., Griesenbach, U., Goussard, S., Gruenert, D., Geddes, D., Scheule, R., Cheng, S., Courvalin, P., Grillot-Courvalin, C., & Alton, E. (2008). Bactofection of lung epithelial cells in vitro and in vivo using a genetically modified *Escherichia coli*. *Gene Ther.*, **15**(6), 434-42.

16. van Pijkeren, J., Morrissey, D., Monk, I., Cronin, M., Rajendran, S., O'Sullivan, G., Gahan, C., & Tangney, M. (2010). A novel *Listeria monocytogenes*-based DNA delivery system for cancer gene therapy. *Hum. Gene Ther.*, **21**(4), 405-16.

17. Yazawa, K., Fujimori, M., Nakamura, T., Sasaki, T., Amano, J., Kano, Y., & Taniguchi, S. (2001). Bifidobacterium longum as a delivery system for gene therapy of chemically induced rat mammary tumors. *Breast Cancer Res*. Treat., **66**(2), 165-70.

18. Sizemore, D., Branstrom, A., & Sadoff, J. (1995). Attenuated Shigella as a DNA delivery vehicle for DNA-mediated immunization. *Science*, **270**(5234), 299-302.

19. Zhu, X., Cai, J., Huang, J., Jiang, X., & Ren, D. (2010). The treatment and prevention of mouse melanoma with an oral DNA vaccine carried by attenuated *Salmonella typhimurium*. *J. Immunother.*, **33**(5), 453-60.

20. Grillot-Courvalin, C., Goussard, S., Huetz, F., Ojcius, D., & Courvalin, P. (1998). Functional gene transfer from intracellular bacteria to mammalian cells. *Nat. Biotechnol.*, **16**(9), 862-6.

21. Fajac, I., Grosse, S., Collombet, J., Thevenot, G., Goussard, S., Danel, C., & Grillot-Courvalin, C. (2004). Recombinant *Escherichia coli* as a gene delivery vector into airway epithelial cells. *J Control Release*, **97**(2), 371-81.

22. Castagliuolo, I., Beggiao, E., Brun, P., Barzon, L., Goussard, S., Manganelli, R., Grillot-Courvalin, C., & Palù, G. (2005). Engineered *E. coli* delivers therapeutic genes to the colonic mucosa. *Gene Ther.*, **12**(13), 1070-8.

23. Kelly, J., Rubin, A., Davis, J., Ajo-Franklin, C., Cumbers, J., Czar, M., de Mora, K., Glieberman, A., Monie, D., & Endy, D. (2009). Measuring the activity of BioBrick promoters using an *in vivo* reference standard. *J Biol Eng*, **3**, 4.

24. Marioni, J., Mason, C., Mane, S., Stephens, M., & Gilad, Y. (2008). RNA-seq: an assessment of technical reproducibility and comparison with gene expression arrays. *Genome Res.*, **18**(9), 1509-17.

25. Kalderon, D., Roberts, B., Richardson, W., & Smith, A. (1985). A short amino acid sequence able to specify nuclear location. *Cell*, **39**, 499-509.

26. Isberg, R., & Leong, J. (1990). Multiple beta 1 chain integrins are receptors for invasin, a protein that promotes bacterial penetration into mammalian cells. *Cell*, **60**(5), 861-71.

27. Collazo, C., & Galán, J. (1997). The invasion-associated type-III protein secretion system in *Salmonella*--a review. *Gene*, **192**(1), 51-9.

28. Chang, C., Cheng, W., Chen, S., Kao, M., Chiang, C., & Chao, Y. (2011). Engineering of *Escherichia coli* for targeted delivery of transgenes to HER2/neu-positive tumor cells. *Biotechnol. Bioeng.*, **108**(7), 1662-72.

29. Alonso, A., & García-del Portillo, F. (2004). Hijacking of eukaryotic functions by intracellular bacterial pathogens. *Int. Microbiol.*, **7**(3), 181-91.

30. Isberg, R., & Van Nhieu, G. (2004). The mechanism of phagocytic uptake promoted by invasin-integrin interaction. *Trends Cell Biol.*, **5**(3), 120-4.

31. Anderson, J., Clarke, E., Arkin, A., & Voigt, C. (2005). Environmentally controlled invasion of cancer cells by engineered bacteria. *J. Mol. Biol.*, **355**(4), 619-27.

32. Lejona, S., Aguirre, A., Cabeza, M., García Véscovi, E., & Soncini, F. (2003). Molecular characterization of the $Mg2^{+}$-responsive PhoP-PhoQ regulon in *Salmonella enterica*. *J. Bacteriol.*, **185**(21), 6287-94.

33. Kato, A., Tanabe, H., & Utsumi, R. (1999). Molecular characterization of the PhoP-PhoQ two-component system in *Escherichia coli* K-12: identification of extracellular $Mg2^{+}$-responsive promoters. *J. Bacteriol.*, **181**(17), 5516-20.

34. Monsieurs, P., De Keersmaecker, S., Navarre, W., Bader, M., De Smet, F., McClelland, M., Fang, F., De Moor, B., Vanderleyden, J., & Marchal, K. (2005). Comparison of the PhoPQ regulon in *Escherichia coli* and *Salmonella typhimurium*. *J. Mol. Evol.*, **60**(4), 462-74.

35. Ernst, R., Guina, T., & Miller, S. (1999). How intracellular bacteria survive: surface modifications that promote resistance to host innate immune responses. *J. Infect. Dis.*, S326-30.

36. García Véscovi, E., Soncini, F., & Groisman, E. (1996). $Mg2^{+}$ as an extracellular signal: environmental regulation of *Salmonella* virulence. *Cell*, **84**(1), 165-74.

37. Young, I., Wang, I., & Roof, W. (2000). Phages will out: strategies of host cell lysis. *Trends Microbiol.*, **8**(3), 120-8.

38. Young, R. (2001). Bacteriophage holins: deadly diversity. *J. Mol. Microbiol. Biotechnol.*, **4**(1), 21-36.

39. Zhang, N., & Young, R. (2000). Complementation and characterization of the nested Rz and Rz1 reading frames in the genome of bacteriophage lambda. *Mol. Gen. Genet.*, **262**, 659-67.

40. Wagner, E., Plank, C., Zatloukal, K., Cotten, M., & Birnstiel, M. (1992). Influenza virus hemagglutinin HA-2 N-terminal fusogenic peptides augment gene transfer by transferrin-polylysine-DNA complexes: toward a synthetic virus-like gene-transfer vehicle. *Proc. Natl. Acad. Sci. U.S.A.*, **89**(17), 7934-8.

41. Greber, U., Willetts, M., Webster, P., & Helenius, A. (1993). Stepwise dismantling of adenovirus 2 during entry into cells. *Cell*, **75**(3), 477-86.

42. Ledley, F. (1996). Nonviral gene therapy: the promise of genes as pharmaceutical products. *Hum. Gene Ther.*, **6**(9), 1129-44.

43. O'Brien, D., & Melville, S. (2004). Effects of Clostridium perfringens alpha-toxin (PLC) and perfringolysin O (PFO) on cytotoxicity to macrophages, on escape from the phagosomes of macrophages, and on persistence of C. perfringens in host tissues. *Infect. Immun.*, **72**(9), 5204-15.

44. Smith, G., Marquis, H., Jones, S., Johnston, N., Portnoy, D., & Goldfine, H. (1995). The two distinct phospholipases C of *Listeria monocytogenes* have overlapping roles in escape from a vacuole and cell-to-cell spread. *Infect. Immun.*, **63**(11), 4231-7.

45. Mogk, A., Schmidt, R., & Bukau, B. (2007). The N-end rule pathway for regulated proteolysis: prokaryotic and eukaryotic strategies. *Trends Cell Biol.*, **17**(4), 165-72.

46. Luzio, J., Bright, N., & Pryor, P. (2007). The role of calcium and other ions in sorting and delivery in the late endocytic pathway. *Biochem. Soc. Trans.*, **35**, 1088-91.

47. Luirink, J., van der Sande, C., Tommassen, J., Veltkamp, E., De Graaf, F., & Oudega, B. (1986). Effects of divalent cations and of phospholipase A activity on excretion of cloacin DF13 and lysis of host cells. *J. Gen. Microbiol.*, **132**(3), 825-34.

48. van der Wal, F., Koningstein, G., ten Hagen, C., Oudega, B., & Luirink, J. (1998). Optimization of bacteriocin release protein (BRP)-mediated protein release by *Escherichia coli*: random mutagenesis of the pCloDF13-derived BRP gene to uncouple lethality and quasi-lysis from protein release. *Appl. Environ. Microbiol.*, **64**(2), 392-8.

49. Pugsley, A., & Rosenbusch, J. (1981). Release of colicin E2 from *Escherichia coli*. *J. Bacteriol.*, **147**(1), 186-92.

50. Anderson, J., Dueber, J., Leguia, M., Wu, G., Goler, J., Arkin, A., & Keasling, J. (2010). BglBricks: A flexible standard for biological part assembly. *J Biol Eng*, **4**(1), 1.

51. Leguia, M., Brophy, J., Densmore, D., & Anderson, J. (2011). Automated assembly of standard biological parts. *Meth. Enzymol.*, **498**, 363-97.

52. Massachusetts Institute of Technology, 2012. Registry of Standard Biological Parts. Massachusetts, U.S.A.: Massachusetts Institute of Technology. Available from: http://partsregistry.org [Accessed 12 April 2012].

53. Kato, A., & Groisman, E. (2004). Connecting two-component regulatory systems by a protein that protects a response regulator from dephosphorylation by its cognate sensor. *Genes Dev.*, **18**(18), 2302-13.

54. Anisimova, E., Badiakina, A., Vasil'eva, N., & Nesmeianova, M. (2005). Changes in the composition of anionic membrane phospholipids influence the protein secretion and biogenesis of cell envelope in *Escherichia coli*. *Mikrobiologiia*, **74**(2), 179-84.

55. Datsenko, K., & Wanner, B. (2000). One-step inactivation of chromosomal genes in *Escherichia coli* K-12 using PCR products. *Proc. Natl. Acad. Sci. U.S.A.*, **97**(12), 6640-5.

56. Haldimann, A., & Wanner, B. (2001). Conditional-replication, integration, excision, and retrieval plasmid-host systems for gene structure-function studies of bacteria. *J. Bacteriol.*, **183**(21), 6384-93.

57. Lennox, E. (1956). Transduction of linked genetic characters of the host by bacteriophage P1. *Virology*, **1**(2), 190-206.

58. Mizushima, N. (2007). Autophagy: process and function. *Genes Dev*., *21*(22), 2861-73.

59. Ogawa, M., Yoshimori, T., Suzuki, T., Sagara, H., Mizushima, N., & Sasakawa, C. (2005). Escape of intracellular *Shigella* from autophagy. *Science*, **307**(5710), 727-31.

60. Pálffy, R., Gardlík, R., Hodosy, J., Behuliak, M., Resko, P., Radvánský, J., & Celec, P. (2006). Bacteria in gene therapy: bactofection versus alternative gene therapy. *Gene Ther.*, **13**(2), 101-5.

61. Fu, G., Li, X., Hou, Y., Fan, Y., Liu, W., & Xu, G. (2005). *Bifidobacterium longum* as an oral delivery system of endostatin for gene therapy on solid liver cancer. *Cancer Gene Ther.*, **12**(2), 133-40.

62. Li, X., Fu, G., Fan, Y., Liu, W., Liu, X., Wang, J., & Xu, G. (2003). *Bifidobacterium adolescentis* as a delivery system of endostatin for cancer gene therapy: selective inhibitor of angiogenesis and hypoxic tumor growth. *Cancer Gene Ther.*, **10**(2), 105-11.

63. Nemunaitis, J., Cunningham, C., Senzer, N., Kuhn, J., Cramm, J., Litz, C., Cavagnolo, R., Cahill, A., Clairmont, C., & Sznol, M. (2003). Pilot trial of genetically modified, attenuated *Salmonella* expressing the *E. coli* cytosine deaminase gene in refractory cancer patients. *Cancer Gene Ther.*, **10**(10), 737-44.

64. Fox, M., Lemmon, M., Mauchline, M., Davis, T., Giaccia, A., Minton, N., & Brown, J. (1996). Anaerobic bacteria as a delivery system for cancer gene therapy: in vitro activation of 5-fluorocytosine by genetically engineered clostridia. *Gene Ther.*, **3**(2), 173-8.

65. Saltzman, D., Heise, C., Hasz, D., Zebede, M., Kelly, S., Curtiss, R., Leonard, A., & Anderson, P. (2000). Attenuated *Salmonella typhimurium* containing interleukin-2 decreases MC-38 hepatic metastases: a novel anti-tumor agent. *Cancer Biother. Radiopharm.*, **11**(2), 145-53.

66. Celec, P., Gardlík, R., Pálffy, R., Hodosy, J., Stuchlík, S., Drahovská, H., Stuchlíková, M., Minárik, G., Lukács, J., Jurkovicová, I., Hulín, I., Turna, J., Jakubovský, J., Kopáni, M., Danisovic, L., Jandzík, D., Kúdela, M., & Yonemitsu, Y. (2004). The use of transformed *Escherichia coli* for experimental angiogenesis induced by regulated in situ production of vascular endothelial growth factor--an alternative gene therapy. *Med. Hypotheses*, **64**(3), 505-11.

67. Liu, S., Minton, N., Giaccia, A., & Brown, J. (2002). Anticancer efficacy of systemically delivered anaerobic bacteria as gene therapy vectors targeting tumor hypoxia/necrosis. *Gene Ther.*, **9**(4), 291-6.

68. Pugsley, A. (1993). The complete general secretory pathway in gram-negative bacteria. *Microbiol. Rev.*, **57**(1), 50-108.

69. Barrett, C., Ray, N., Thomas, J., Robinson, C., & Bolhuis, A. (2003). Quantitative export of a reporter protein, GFP, by the twin-arginine translocation pathway in *Escherichia coli*. *Biochem. Biophys. Res. Commun.*, **304**(2), 279-84.

70. Feilmeier, B., Iseminger, G., Schroeder, D., Webber, H., & Phillips, G. (2000). Green fluorescent protein functions as a reporter for protein localization in *Escherichia coli*. *J. Bacteriol.*, **182**(14), 4068-76.

71. Park, T., Struck, D., Dankenbring, C., & Young, R. (2007). The pinholin of lambdoid phage 21: control of lysis by membrane depolarization. *J. Bacteriol.*, **189**(24), 9135-9.

72. King, N., Westbrook, M., Young, S., Kuo, A., Abedin, M., Chapman, J., Fairclough, S., Hellsten, U., Isogai, Y., Letunic, I., Marr, M., Pincus, D., Putnam, N., Rokas, A., Wright, K., Zuzow, R., Dirks, W., Good, M., Goodstein, D., Lemons, D., Li, W., Lyons, J., Morris, A., Nichols, S., Richter, D., Salamov, A., Sequencing, J., Bork, P., Lim, W., Manning, G., Miller, W., McGinnis, W., Shapiro, H., Tjian, R., Grigoriev, I., & Rokhsar, D. (2008). The genome of the choanoflagellate *Monosiga brevicollis* and the origin of metazoans. *Nature*, **451**(7180), 783-8.

73. Pincus, D., Letunic, I., Bork, P., & Lim, W. (2008). Evolution of the phospho-tyrosine signaling machinery in premetazoan lineages. *Proc. Natl. Acad. Sci. U.S.A.*, **105**(28), 9680-4.

74. Fairclough, S., Dayel, M., & King, N. (2010). Multicellular development in a choanoflagellate. *Curr. Biol.*, **20**(20), R875-6.

75. Nelson, M., & Silver, P. (1989). Context affects nuclear protein localization in *Saccharomyces cerevisiae*. *Mol. Cell. Biol.*, **9**(2), 384-9.

76. Goldfarb, D., Gariépy, J., Schoolnik, G., & Kornberg, R. (1986). Synthetic peptides as nuclear localization signals. *Nature*, **322**(6080), 641-4.

77. Raikhel, N. (2010). Nuclear targeting in plants. *Plant Physiol.*, **100**(4), 1627-32.

78. UC Berkeley iGEM 2010 Team, 2010. Choa Choa's Delivery Service. Massachusetts, U.S.A.: Massachusetts Institute of Technology. Available from: http://2010.igem.org/Team:Berkeley [Accessed 12 April 2012].

79. Waheed, A., Shimada, Y., Heijnen, H., Nakamura, M., Inomata, M., Hayashi, M., Iwashita, S., Slot, J., & Ohno-Iwashita, Y. (2001). Selective binding of perfringolysin O derivative to cholesterol-rich membrane microdomains (rafts). *Proc. Natl. Acad. Sci. U.S.A.*, **98**(9), 4926-31.

80. Fulton, C. (1970). Chapter 13 Amebo-flagellates as Research Partners: The Laboratory Biology of *Naegleria* and *Tetramitus*. *Methods in Cell Biology*, **4**, 341–476.

81. Balbo, A., & Bozzaro, S. (2006). Cloning of *Dictyostelium* eIF6 (p27BBP) and mapping its nucle(ol)ar localization subdomains. *Eur. J. Cell Biol.*, **85**, 1069-78.

82. Myre, M., & O'Day, D. (2002). Nucleomorphin. A novel, acidic, nuclear calmodulin-binding protein from *Dictyostelium* that regulates nuclear number. *J. Biol. Chem.*, **277**(22), 19735-44.

83. Mosammaparast, N., Jackson, K., Guo, Y., Brame, C., Shabanowitz, J., Hunt, D., & Pemberton, L. (2001). Nuclear import of histone H2A and H2B is mediated by a network of karyopherins. *J. Cell Biol.*, **153**(2), 251-62.

84. Riedl, J., Crevenna, A., Kessenbrock, K., Yu, J., Neukirchen, D., Bista, M., Bradke, F., Jenne, D., Holak, T., Werb, Z., Sixt, M., & Wedlich-Soldner, R. (2008). Lifeact: a versatile marker to visualize F-actin. *Nat. Methods*, **5**(7), 605-7.

85. Kapuscinski, J. (1996). DAPI: a DNA-specific fluorescent probe. *Biotech Histochem*, **70**(5), 220-33.

86. Latt, S., & Stetten, G. (1976). Spectral studies on 33258 Hoechst and related bisbenzimidazole dyes useful for fluorescent detection of deoxyribonucleic acid synthesis. *J. Histochem. Cytochem.*, **24**(1), 24-33.

87. Choanoflagellate Research Community, 2012. ChoanoWiki. California, U.S.A.: Choanoflagellate Research Community. Available from: http://www.choano.org/wiki/ChoanoWiki [Accessed 12 April 2012].

88. Lecoeur, H. (2002). Nuclear apoptosis detection by flow cytometry: influence of endogenous endonucleases. *Exp. Cell Res.*, **277**(1), 1-14.

89. SynBERC, 2012. Testbeds. California, U.S.A.: SynBERC. Available from: http://www.synberc.org/testbeds [Accessed 12 April 2012].

90. Singer, E., 2006. Tumor-Killing Bacteria. Massachusetts, U.S.A.: Massachusetts Institute of Technology. Available from: http://www.technologyreview.com/printer_friendly_article.aspx?id=16949 [Accessed 12 April 2012].

91. Anderson, J., Voigt, C., & Arkin, A. (2007). Environmental signal integration by a modular AND gate. *Mol. Syst. Biol.*, **3**, 133.

92. Katsnelson, A., 2010. DNA factory builds up steam. California, U.S.A.: Nature Publishing Group. Available from: http://www.nature.com/news/2010/100722/full/news.2010.367.html [Accessed 12 April 2012].

93. Guzman, L., Belin, D., Carson, M., & Beckwith, J. (1995). Tight regulation, modulation, and high-level expression by vectors containing the arabinose PBAD promoter. *J. Bacteriol.*, **177**(14), 4121-30.

94. Anderson, J. C., 2006. Part:BBa_J23101. Massachusetts, U.S.A.: Massachusetts Institute of Technology. Available from: http://partsregistry.org/wiki/index.php?title=Part:BBa_J23101 [Accessed 12 April 2012].

95. Huh, J., 2012. Part:BBa_J72131. Massachusetts, U.S.A.: Massachusetts Institute of Technology. Available from: http://partsregistry.org/Part:BBa_J72131 [Accessed 12 April 2012].

96. Rhee, J., Tao, C., Thomson, T., & Waldman, L., 2006. Part:BBa_R0040. Massachusetts, U.S.A.: Massachusetts Institute of Technology. Available from: http://partsregistry.org/Part:BBa_R0040 [Accessed 12 April 2012].

97. Shetty, R., 2003. Part:BBa_B0015. Massachusetts, U.S.A.: Massachusetts Institute of Technology. Available from: http://partsregistry.org/Part:BBa_B0015 [Accessed 12 April 2012].

98. Anderson, J. C., 2007. Part:BBa_J61048. Massachusetts, U.S.A.: Massachusetts Institute of Technology. Available from: http://partsregistry.org/Part:BBa_J61048 [Accessed 12 April 2012].

99. Huang, H., 2006. Part:BBa_B1006. Massachusetts, U.S.A.: Massachusetts Institute of Technology. Available from: http://partsregistry.org/Part:BBa_B1006 [Accessed 12 April 2012].

100. Bustamante, V., Villalba, M., García-Angulo, V., Vázquez, A., Martínez, L., Jiménez, R., & Puente, J. (2011). PerC and GrlA independently regulate Ler expression in enteropathogenic *Escherichia coli*. *Mol. Microbiol.*, **82**(2), 398-415.

101. Libby, S., Lesnick, M., Hasegawa, P., Kurth, M., Belcher, C., Fierer, J., & Guiney, D. (2002). Characterization of the spv locus in *Salmonella enterica* serovar Arizona. *Infect. Immun.*, **70**(6), 3290-4.

102. Neufing, P., Shearwin, K., Camerotto, J., & Egan, J. (1997). The CII protein of bacteriophage 186 establishes lysogeny by activating a promoter upstream of the lysogenic promoter. *Mol. Microbiol.*, **21**(4), 751-61.

103. Lei, S., Lin, H., Wang, S., Callaway, J., & Wilcox, G. (1987). Characterization of the *Erwinia carotovora* pelB gene and its product pectate lyase. *J. Bacteriol.*, **169**(9), 4379-83.

104. McKnight, C., Briggs, M., & Gierasch, L. (1989). Functional and nonfunctional LamB signal sequences can be distinguished by their biophysical properties. *J. Biol. Chem.*, **264**(29), 17293-7.

105. Ignatova, Z., Hörnle, C., Nurk, A., & Kasche, V. (2002). Unusual signal peptide directs penicillin amidase from *Escherichia coli* to the Tat translocation machinery. *Biochem. Biophys. Res. Commun.*, **291**(1), 146-9.

106. White, R., Chiba, S., Pang, T., Dewey, J., Savva, C., Holzenburg, A., Pogliano, K., & Young, R. (2011). Holin triggering in real time. *Proc. Natl. Acad. Sci. U.S.A.*, **108**(2), 798-803.

107. Tran, T., Struck, D., & Young, R. (2005). Periplasmic domains define holin-antiholin interactions in T4 lysis inhibition. *J. Bacteriol.*, **187**(19), 6631-40.

108. Canton, B., Labno, A., & Endy, D. (2008). Refinement and standardization of synthetic biological parts and devices. *Nat. Biotechnol.*, **26**(7), 787-93.

109. Kim, E., & Wyckoff, H. (1991). Reaction mechanism of alkaline phosphatase based on crystal structures. Two-metal ion catalysis. *J. Mol. Biol.*, **218**(2), 449-64.

110. Pédelacq, J., Cabantous, S., Tran, T., Terwilliger, T., & Waldo, G. (2006). Engineering and characterization of a superfolder green fluorescent protein. *Nat. Biotechnol.*, **24**(1), 79-88.

111. Registry of Standard Biological Parts, 2012. Part: BBa_E1010. Massachusetts, U.S.A.: Massachusetts Institute of Technology. Available from: http://partsregistry.org/Part: BBa_E1010 [Accessed 12 April 2012].

112. Huh, J., 2012. Part:BBa_J72131. Massachusetts, U.S.A.: Massachusetts Institute of Technology. Available from: http://partsregistry.org/Part:BBa_J72131 [Accessed 12 April 2012].

113. Wong, K., & Kwan, H. (1992). Transcription of glpT of *Escherichia coli* K12 is regulated by anaerobiosis and fnr. *FEMS Microbiol. Lett.*, **73**, 15-8.

114. Tullman-Ercek, D., DeLisa, M., Kawarasaki, Y., Iranpour, P., Ribnicky, B., Palmer, T., & Georgiou, G. (2007). Export pathway selectivity of *Escherichia coli* twin arginine translocation signal peptides. *J. Biol. Chem.*, **282**(11), 8309-16.

115. Registry of Standard Biological Parts, 2012. Part: BBa_K082003. Massachusetts, U.S.A.: Massachusetts Institute of Technology. Available from: http://partsregistry.org/Part: BBa_K082003 [Accessed 12 April 2012].

116. Meissner, D., Vollstedt, A., van Dijl, J., & Freudl, R. (2007). Comparative analysis of twin-arginine (Tat)-dependent protein secretion of a heterologous model protein (GFP) in three different Gram-positive bacteria. *Appl. Microbiol. Biotechnol.*, **76**(3), 633-42.

Appendix

Table 1. List of Basic Parts

Key:

rbs_sfGFP! ribosome binding site (rbs) before and stop codon after the coding sequence (CDS) of sfGFP
<sfGFP! rbs and start codon are not present, stop codon after the CDS
<sfGFP> no rbs, start codon, or stop codon

Registry #	Name	Description/Source
BBa_J72045	P_{BAD}	Arabinose inducible promoter from *E. coli* [93]
BBa_J72047	P_{REF}	BglBrick standard version of Bba_J23101, Synthetic constitutive promoter [94]
BBa_J72131	P_{CON}-B5	Synthetic constitutive promoter in BBa format [95]
BBa_J72050	P_{CON}-B5	BglBrick standard version of BBa_J72131
BBa_J72005	P_{TET}	BglBrick standard version of BBa_R0040 ,TetR repressible promoter [96]
BBa_B0015	double terminator	Transcription terminator in BBa format [97]
BBa_J72049	double terminator	BglBrick standard version of Bba_B0015
BBa_J61048	*rnpB* terminator	Transcription terminator in BBa format [98]
BBa_J72051	*rnpB* terminator	BglBrick standard version of Bba_J61048
BBa_J72059	terminator	BglBrick standard version of BBa_B1006, synthetic transcription terminator [99]
BBa_J72052	rbs_*brp*!	A modified version of bacteriocin release protein from *E. coli* [48]
BBa_J72053	P_{mgtCB}	Mg^{2+} responsive promoter from *Salmonella enterica* [32]
BBa_J72054	P_{phoP}	Mg^{2+} responsive promoter from *E. coli* [33]
BBa_J72055	P_{mgtCBI}	Mg^{2+} responsive promoter from *Salmonella enterica* [32]
BBa_J72056	P_{mgrBI}	Mg^{2+} responsive promoter from *E. coli* [33]
BBa_J72057	P_{mgtA}	Mg^{2+} responsive promoter from *E. coli* [33]
BBa_J72058	rbs_*perC2*!	Activator of P_{ler314}. From enteropathogenic *E. coli* (EPEC) [100]
BBa_J72060	P_{ler314}	Promoter activated by rbs_perC2!. From enteropathogenic *E. coli* (EPEC) [100]
BBa_J72061	rbs_*spvR*!	Activator of P_{spv2}. From *Salmonella enterica* [101]
BBa_J72062	P_{spv2}	Promoter activated by rbs_spvR!. From

		Salmonella enterica [101]
BBa_J72063	rbs_*186-cII*!	Activator of P_{pEI}. From Coliphage 186 [102]
BBa_J72064	P_{pEI}	Promoter activated by rbs_186-cII!. From Coliphage 186 [102]
BBa_J72065	rbs_*pelB*>	Leader sequence of pelB from *Erwinia carotovora* CE [103]
BBa_J72066	rbs_*pelB*_R>	Leader sequence that exposes Arg at N-terminus after cleavage [45]. From *Erwinia carotovora* CE [103]
BBa_J72067	rbs_*lamB*>	Leader sequence of lamB from *E. coli* [104]
BBa_J72068	rbs_*lamB*_R>	Leader sequence of lamB that expose Arg at N-terminus after cleavage [45]. From *E. coli* [104]
BBa_J72069	rbs_*ompT*_stR>	Leader sequence of ompT that expose Arg at N-terminus after cleavage [45]. From *E. coli* [105]
BBa_K112305	rbs_lLysozyme!	Lysozyme from enterobacteria phage λ [106]
BBa_K112311	rbs_lholin!	Holin from enterobacteria phage λ [106]
BBa_K112317	rbs_lantiholin!	Antiholin from enterobacteria phage λ [106]
BBa_J72123	rbs_tLysozyme!	Lysozyme from enterobacteria phage T4 in BBa format [107]
BBa_J72124	rbs_tholin!	Holin from enterobacteria phage T4 in BBa format [107]
BBa_J72125	rbs_tantiholin!	Antiholin from enterobacteria phage T4 in BBa format [107]
BBa_K112408	rbs_tholin!.b0015.P_{CON}.rbs_tantiholin!.*rnpB*T	Composite part consisting of BBa_J72123.BBa_J72124.BBa_B0015.BBa_J72131,BBa_J72125.BBa_J61048 assembled in BBa format [108], converted into a BglBrick standard basic part.
BBa_J72126	<PI-*plc*!	Phosphoinositide-specific phospholipase C (*plcA*) from *Listeria monocytogenes* [44]
BBa_J72127	<PC-*plc*!	Phosphatidylcholine-specific phospholipase C (*plcB*) from *Listeria monocytogenes* [44]
BBa_J72128	< *plc*!	Phospholipase C (*plc*) from *Clostridium perfringens* [43]
BBa_J72129	<*pfo*!	Perfringolysin O (*pfo*) from *Clostridium perfringens* [43]
BBa_J72130	P_{flu}-Inv	Invasin *(Inv)* from *Yersinia pseudotuberculosis* [31]
BBa_J72119	P_{CON}.*phoA*	Constitutively expressed alkaline phosphatase from *E. coli* [109]
BBa_J72120	rbs_sfGFP>	Superfolder GFP with no stop codon from *Aequorea victoria* [110]
BBa_J72048	rbs_sfGFP!	Superfolder green fluorescent protein from *Aequorea victoria* [110]
BBa_J72122	rbs_RFP!	BglBrick standard version of BBa_E1010, red fluorescent protein [111]
BBa_J72121	<NLS!	Nucleus localization signal from SV40 without start codon [25]

BBa_J72139	P_{CON}-J23102	Synthetic constitutive promoter in BBa format [112]
BBa_J72140	P_{glpT}	Promoter expressed under anaerobic growth conditions [113]
BBa_J72142	rbs_ycbKss>	Leader sequence of torA from *E. coli* [114]
BBa_J72143	<GFP-LVA>	BglBrick standard version of BBa_K082003 without start and stop codons [115]
BBa_J72144	rbs_torAss2>	Leader sequence of torA from *E. coli* [116]
BBa_J72145	<RFP!	BglBrick standard version of BBa_E1010, red fluorescent protein with no start codon [111]
BBa_J72117	pBca1256	Synthetic high copy number SpecR plasmid backbone with ColE1 origin
BBa_J72118	pBjh1601CA	Synthetic medium copy number CamR/AmpR plasmid backbone with p15A origin
BBa_J72146	pBjk2807	Synthetic SpecR plasmid backbone with R6K origin
BBa_J72147	pBjk2741	Synthetic SpecR plasmid backbone with ColE2 origin
BBa_J72148	pBth7034C	Synthetic medium copy number CamR plasmid backbone with ColE1 origin

Table 2. List of Composite Parts

Key:

BBa_J72045.BBa_J72046 BBa_J72045 assembled with BBa_J72046

Name	Description	Composition
Bjh1849	Invasion Device	BBa_J72130
Bjh2313	Payload Device	BBa_J72005.BBa_J72120.BBa_J72121.BBa_J72122.BBa_J72049
Bjh2366	P_{BAD} driven GFP	BBa_J72045.BBa_J72048.BBa_J72049
Bjh2302	P_{REF} driven GFP	BBa_J72047.BBa_J72048.BBa_J72049
Bxa160	P_{BAD} driven SLD(λ)	BBa_J72045.BBa_K112305.BBa_K112311.BBa_J72049.BBa_J72050.BBa_K112317.BBa_J72051
Bjh1998	P_{BAD} driven SLD(T4)	BBa_J72045.BBa_K112408
Bjh1968	P_{BAD} driven SLD(λ) with BRP	BBa_J72045.BBa_J72052.BBa_K112305.BBa_K112311.BBa_J72049.BBa_J72050.BBa_K112317.BBa_J72051
Bjh2389	VSD(P_{mgtCB}) driven GFP	BBa_J72053.BBa_J72048.BBa_J72049
Bjh2297	VSD(P_{phoP}) driven GFP	BBa_J72054.BBa_J72048.BBa_J72049
Bjh2387	VSD(P_{mgtCBI}) driven GFP	BBa_J72055.BBa_J72048.BBa_J72049
Bjh2386	VSD(P_{mgrBI}) driven GFP	BBa_J72056.BBa_J72048.BBa_J72049
Bjh2388	VSD(P_{mgtA}) driven GFP	BBa_J72057.BBa_J72048.BBa_J72049.
Bjh2298	VSD(P_{phoP}-Act4) driven GFP	BBa_J72054.BBa_J72058.BBa_J72059.BBa_J72060.BBa_J72048.BBa_J72049
Bjh2299	VSD(P_{phoP}-Act1) driven GFP	BBa_J72054.BBa_J72061.BBa_J72059.BBa_J72062.BBa_J72048.BBa_J72049
Bjh2300	VSD(P_{phoP}-Act3) driven GFP	BBa_J72054.BBa_J72063.BBa_J72059.BBa_J72064.BBa_J72048.BBa_J72049
Bjh2325	VSD(P_{phoP}-Act2) driven GFP	BBa_J72054.BBa_J72058.BBa_J72060.BBa_J72048.BBa_J72049
Bjh1236	VSD(P_{mgtCB}) driven SLD(λ)	BBa_J72053.BBa_K112305.BBa_K112311.BBa_J72049.BBa_J72050.BBa_K112317.BBa_J72051
Bjh1239	VSD(P_{phoP}) driven SLD(λ)	BBa_J72054.BBa_K112305.BBa_K112311.BBa_J72049.BBa_J72050.BBa_K112317.BBa_J72051
Bjh1242	VSD(P_{mgtCBI}) driven SLD(λ)	BBa_J72055.BBa_K112305.BBa_K112311.BBa_J72049.BBa_J72050.BBa_K112317.BBa_J72051
Bjh2369	VSD(P_{mgrBI}) driven	BBa_J72056.BBa_K112305.BBa_K112311.BB

	SLD(λ)	a_J72049.BBa_J72050.BBa_K112317.BBa_J72051
Bjh2370	VSD(P_{mgtA}) driven SLD(λ)	BBa_J72057.BBa_K112305.BBa_K112311.BBa_J72049.BBa_J72050.BBa_K112317.BBa_J72051
Bjh2371	VSD($P_{phoP\text{-}Act4}$) driven SLD(λ)	BBa_J72054.BBa_J72058.BBa_J72059.BBa_J72060.BBa_K112305.BBa_K112311.BBa_J72049.BBa_J72050.BBa_K112317.BBa_J72051
Bjh2372	VSD($P_{phoP\text{-}Act1}$) driven SLD(λ)	BBa_J72054.BBa_J72061.BBa_J72059.BBa_J72062.BBa_K112305.BBa_K112311.BBa_J72049.BBa_J72050.BBa_K112317.BBa_J72051
Bjh2373	VSD($P_{phoP\text{-}Act3}$) driven SLD(λ)	BBa_J72054.BBa_J72063.BBa_J72059.BBa_J72064.BBa_K112305.BBa_K112311.BBa_J72049.BBa_J72050.BBa_K112317.BBa_J72051
Bjh2374	VSD($P_{phoP\text{-}Act2}$) driven SLD(λ)	BBa_J72054.BBa_J72058.BBa_J72060.BBa_J72060.BBa_K112305.BBa_K112311.BBa_J72049.BBa_J72050.BBa_K112317.BBa_J72051
Bjh2109	P_{BAD}-*brp* expression plasmid	BBa_J72045.BBa_J72052.BBa_J72049
Bjh2143c12	constitutive PhoA expression plasmid	BBa_J72119
Bjh1874	VSD(P_{phoP}) driving SLD(λ) with BRP	BBa_J72054.BBa_J72052.BBa_K112305.BBa_K112311.BBa_J72049.BBa_J72050.BBa_K112317.BBa_J72051
Bjh1865	VSD(P_{phoP}) driving SLD(λ) with BRP and VLD(*pfo*)	BBa_J72054.BBa_J72065. BBa_J72129.BBa_J72052.BBa_K112305.BBa_K112311.BBa_J72049.BBa_J72050.BBa_K112317.BBa_J72051
Bjh1866	VSD(P_{phoP}) driving SLD(λ) with BRP and VLD (degradation tagged *pfo*)	BBa_J72054.BBa_J72066. BBa_J72129.BBa_J72052.BBa_K112305.BBa_K112311.BBa_J72049.BBa_J72050.BBa_K112317.BBa_J72051
Bjh1864	VSD(P_{phoP}) driving SLD(λ) with BRP and VLD(*pfo*, *plc*)	BBa_J72054.BBa_J72065. BBa_J72129.BBa_J72067. BBa_J72128.BBa_J72052.BBa_K112305.BBa_K112311.BBa_J72049.BBa_J72050.BBa_K112317.BBa_J72051
Bjh1872	VSD(P_{phoP}) driving SLD(λ) with BRP and VLD(degradation tagged *pfo* and *plc*)	BBa_J72054.BBa_J72066. BBa_J72129.BBa_J72068. BBa_J72128.BBa_J72052.BBa_K112305.BBa_K112311.BBa_J72049.BBa_J72050.BBa_K112317.BBa_J72051
Bjh2268	VSD(P_{phoP}) driving	BBa_J72054.BBa_J72066.PFO.BBa_J72069.

	SLD(λ) with BRP and VLD (degradation tagged *pfo*, *plcA*, and *plcB*)	BBa_J72126.BBa_J72068. BBa_J72127.BBa_J72052.BBa_K112305.BBa_K112311.BBa_J72049.BBa_J72050.BBa_K112317.BBa_J72051
Bjh2348	PDD with P_{CON} driving VLD(degradation tagged *pfo*/*plc*) and VSD(P_{phoP}) driving SLD(λ) with BRP	BBa_J72054.BBa_J72052.BBa_K112305.BBa_K112311.BBa_J72049.BBa_J72050.BBa_K112317.BBa_J72051.BBa_J72005.BBa_J72066. BBa_J72129.BBa_J72068. BBa_J72128.BBa_J72059
Bjh2399	PDD with P_{CON} driving VLD(degradation tagged *pfo*/*plc*) and VSD(P_{mgrBl}) driving a SLD(λ) with BRP	BBa_J72056.BBa_J72052.BBa_K112305.BBa_K112311.BBa_J72049.BBa_J72050.BBa_K112317.BBa_J72051.BBa_J72005.BBa_J72066. BBa_J72129.BBa_J72068. BBa_J72128.BBa_J72059
Bjh2400	PDD with P_{CON} driving VLD(degradation tagged *pfo*/*plc*) and VSD(P_{mgtCBl}) driving a SLD(λ) with BRP	BBa_J72055.BBa_J72052.BBa_K112305.BBa_K112311.BBa_J72049.BBa_J72050.BBa_K112317.BBa_J72051.BBa_J72070.BBa_J72066.BBa_J72129.BBa_J72068.BBa_J72128.BBa_J72059
Bca1144	P_{CON} driven RFP	BBa_J72005.BBa_J72122.BBa_J72049
Bjh2107	VSD(P_{phoP}) driving VLD(degradation tagged *pfo*/*plc*) and BRP, and P_{CON} driving TAT tagged PLD	BBa_J72054.BBa_J72066.BBa_J72129.BBa_J72068.BBa_J72128.BBa_J72052.BBa_J72059.BBa_J72005.BBa_J72142. BBa_J72143.BBa_J72121.BBa_J72144.BBa_J72145.BBa_J72059
Bjh2131	VSD(P_{mgrBl}) driving IMP with BRP	BBa_J72054.BBa_J72052.BBa_K112311.BBa_J72049.BBa_J72050.BBa_K112317.BBa_J72051
Bjh2402	PSD with P_{CON} driving VLD(degradation tagged *pfo*/*plc*), and VSD(P_{mgrBl}) driving IMP with BRP	BBa_J72056.BBa_J72052.BBa_K112311.BBa_J72049.BBa_J72050.BBa_K112317.BBa_J72051.BBa_J72070.BBa_J72066.BBa_J72129. BBa_J72068.BBa_J72128.BBa_J72059
Bjh2347	PSD with P_{CON} driving VLD(degradation tagged *pfo*/*plc*), and VSD(P_{phoP}) driving IMP with BRP	BBa_J72054.BBa_J72052.BBa_K112311.BBa_J72049.BBa_J72050.BBa_K112317.BBa_J72051.BBa_J72070.BBa_J72066.BBa_J72129. BBa_J72068.BBa_J72128.BBa_J72059
Bjh2087	PSD with P_{phoP} driving VLD(degradation tagged *pfo*/*plc*),	BBa_J72054.BBa_J72066.BBa_J72129.BBa_J72068.BBa_J72128.BBa_J72052.BBa_K112311.BBa_J72049.BBa_J72050.BBa_K112317. BBa_J72051

	IMP, and BRP	
jtk2828	P_{glpT} driving GFP	BBa_J72140.BBa_J72048
HK42	VSD(P_{mgrBl}) driving BRP, and P_{BAD} driving VLD(degradation tagged *pfo*/*plc*)	BBa_J72056.BBa_J72052.BBa_J72059.BBa_J72045.BBa_J72066.BBa_J72129.BBa_J72068.BBa_J72128.BBa_J72059
HK45	VSD(P_{mgrBl}) driving BRP, and P_{RHM} driving VLD(degradation tagged *pfo*/*plc*)	BBa_J72056.BBa_J72052.BBa_J72059.{rhaRS_PrhaB}.BBa_J72066.BBa_J72129.BBa_J72068.BBa_J72128.BBa_J72059
HK54	P_{BAD} driven GFP, and P_{CON} driven RFP	BBa_J72045.BBa_J72120.BBa_J72121.BBa_J72059.BBa_J72050.BBa_J72122.BBa_J72059
HK63	P_{BAD} driving IMP with BRP, and P_{CON} driven RFP	BBa_J72045.BBa_J72052.BBa_K112311.BBa_J72049.BBa_J72050.BBa_K112317.BBa_J72051.BBa_J72139.BBa_J72120.BBa_J72121.BBa_J72059